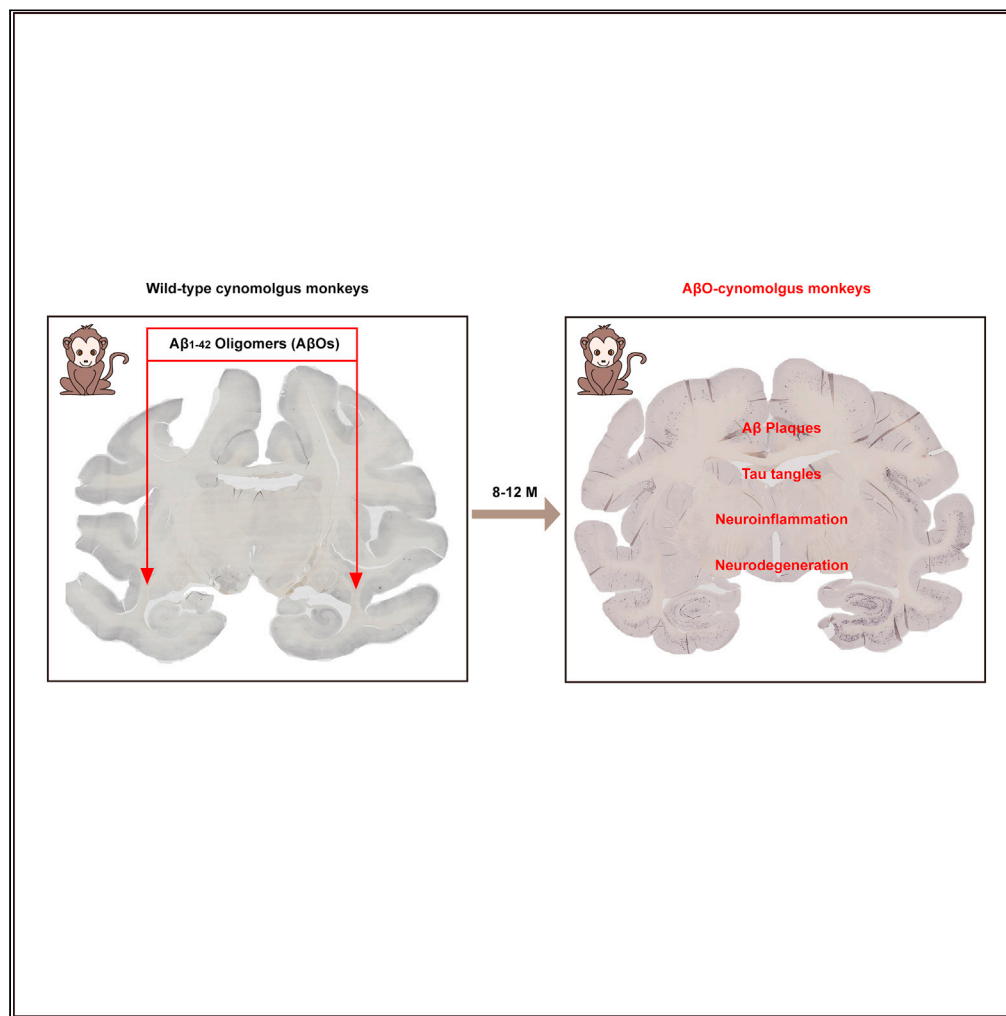


## Article

Synthetic amyloid- $\beta$  oligomers drive early pathological progression of Alzheimer's disease in nonhuman primates

Feng Yue, Su  
Feng, Chunling  
Lu, ..., Jing Liu,  
Chunmei Yue,  
Naihe Jing

fyuee@hotmail.com (F.Y.)  
cmyue@sibcb.ac.cn (C.Y.)  
njing@sibcb.ac.cn (N.J.)

**Highlights**

The A $\beta$  oligomers (A $\beta$ Os) drive to develop massive A $\beta$  plaque in the monkey brain

Neurofibrillary tangles form in multiple brain regions of A $\beta$ O-monkeys

The co-occurrence of amyloid and tau pathology in A $\beta$ O-monkeys as in patients with AD

The neuroinflammation and neurodegeneration are triggered in A $\beta$ O-monkeys

## Article

Synthetic amyloid- $\beta$  oligomers drive early pathological progression of Alzheimer's disease in nonhuman primatesFeng Yue,<sup>1,2,11,\*</sup> Su Feng,<sup>3,4,11</sup> Chunling Lu,<sup>5,11</sup> Ting Zhang,<sup>3,6,7,11</sup> Guoxian Tao,<sup>5</sup> Jing Liu,<sup>4</sup> Chunmei Yue,<sup>3,8,\*</sup> and Naihe Jing<sup>3,4,9,10,12,\*</sup>

## SUMMARY

**As an insidious and slowly progressive neurodegenerative disorder, Alzheimer's disease (AD) uniquely develops in humans but fails in other species. Therefore, it has been challenged to rebuild human AD in animals, including in non-human primates. Here, we bilaterally delivered synthetic A $\beta$  oligomers (A $\beta$ O) into the cerebral parenchyma of cynomolgus monkeys, which rapidly drove the formation of massive A $\beta$  plaques and concomitant neurofibrillary tangles in the cynomolgus brain. The amyloid and tau pathology as well as their co-occurrence in A $\beta$ O-monkeys were reminiscent of those in patients with AD. In addition, the activated astrocytes and microglia surrounding A $\beta$  plaques indicated the triggered neuroinflammation. The degenerative neurons and synapses around A $\beta$  plaques also emerged in cynomolgus brain. Together, soluble A $\beta$ O caused the cascade of pathologic events associated with AD in monkeys as occurred in patients at the early phase, which could facilitate the development of a promising animal model for human AD in non-human primates.**

## INTRODUCTION

Being an aging-related neurodegenerative disorder, Alzheimer's disease (AD) is characterized by  $\beta$ -amyloid (A $\beta$ ) plaques and neurofibrillary tangles at early stages and neuronal loss at late stages. Owing to the biological changes and environmental influences, such as genetics, epigenetics, lifespan, and metabolism, humans are extremely susceptible to AD (Rosen et al., 2016; Walker and Jucker, 2017). In general, other species, such as rodents, are naturally resistant to develop AD even as they grow old. Currently, AD is considered a multifactorial syndrome that is unique to humans and hard to replicate in other species. The various lines of AD mice that have been widely used fail to fully reproduce AD-associated pathological features, such as neurofibrillary tangles (Drummond and Wisniewski, 2017; LaFerla and Green, 2012). The generation of an appropriate mouse model to authentically recapitulate pathological hallmarks of human AD has still proven challenging. Consequently, the understanding of the neuropharmacology, biochemistry, and molecular biology of AD that relied heavily on animal models has been hampered.

It has been well documented that non-human primates share the closest similarity with humans in terms of genetics, brain structure and function, and lifespan (Serenio and Tootell, 2005). The cynomolgus monkey (*Macaca fascicularis*) shares 100% sequence homology of amyloid precursor protein (APP) 695, and of course A $\beta$  40/42 peptides, with humans (Podlisny et al., 1991). In particular, some aged primate species naturally display age-related changes that are reminiscent of AD, such as A $\beta$  plaques (Cramer et al., 2018; Edler et al., 2017; Oikawa et al., 2010; Selkoe et al., 1987). Therefore, non-human primates possess distinct suitability in reproducing AD pathological changes that no other animal species have provided. Re-building the AD-like conditions in primate species might yield more informative clues that triggered this human unique brain disorder.

Previous studies showed that the injection of brain homogenates or A $\beta$  fibrillar from patients with AD caused scattered A $\beta$  deposits near injection sites in the cortex of aged rhesus or marmosets (Baker et al., 1993; Geula et al., 1998). However, tau tangle was not detected in these monkeys with AD brain homogenates or insoluble A $\beta$  fibrillar. Later on, A $\beta$  oligomers (A $\beta$ O), small soluble and diffusible ligands derived from A $\beta$  peptides, were identified as the most potent neurotoxins in AD brain and played a pivotal

<sup>1</sup>School of Biomedical Engineering, Hainan University, Haikou, 570228, China

<sup>2</sup>Department of Neurobiology, Beijing Institute of Geriatrics, Xuanwu Hospital of Capital Medical University, Beijing, 100053, China

<sup>3</sup>State Key Laboratory of Cell Biology, CAS Center for Excellence in Molecular Cell Science, Shanghai Institute of Biochemistry and Cell Biology, Chinese Academy of Sciences; University of Chinese Academy of Sciences, Shanghai, 200031, China

<sup>4</sup>Bioland Laboratory (Guangzhou Regenerative Medicine and Health Guangdong Laboratory), Guangzhou, 510005, China

<sup>5</sup>Wincon TheraCells Biotechnologies Co, LTD, Nanning, 530000, China

<sup>6</sup>Department of Ophthalmology, Shanghai General Hospital, Shanghai Jiao Tong University, School of Medicine, Shanghai Key Laboratory of Ocular Fundus Diseases, Shanghai Engineering Center for Visual Science and Photomedicine, Shanghai, 200080, China

<sup>7</sup>National Clinical Research Center for Ophthalmic Diseases, Shanghai, 200080, China

<sup>8</sup>Department of Biological Sciences, School of Science, Xi'an Jiaotong-Liverpool University, Suzhou, 215000, China

<sup>9</sup>CAS Key Laboratory of Regenerative Biology, Guangdong Provincial Key Laboratory of Stem Cell and Regenerative Medicine, Guangzhou Institutes of Biomedicine and Health, Chinese Academy of

Continued



role in AD pathogenesis (Haass and Selkoe, 2007; Shankar et al., 2008; Viola and Klein, 2015; Walsh et al., 2000). Subsequently, extensive evidence confirmed that soluble A $\beta$ O s rapidly stimulated tau phosphorylation *in vitro* and induced neuron degeneration as well as synapse loss in the brain of mouse and rat (Brouillette et al., 2012; De Felice et al., 2008; Lambert et al., 1998; Lesné et al., 2006; Malm et al., 2006). However, the attempts to test the effects of soluble A $\beta$ O s in non-human primates *in vivo* have been sparse. Several years ago, a report has showed that delivering soluble A $\beta$ O s into the lateral ventricles of macaques caused tau hyperphosphorylation but failed to induce the formation of A $\beta$  plaques in the monkey brain (Fornly-Germano et al., 2014). Other than that, the neurofibrillary-like structures detected in these macaques were morphologically different from those in patients (Fornly-Germano et al., 2014). Recently, the same procedures performed in rhesus monkeys still failed to induce the amyloid plaques and tau pathology, which only caused the loss of dendritic spines similar to that observed in normal aged monkeys (Beckman et al., 2019). Therefore, it remains largely uncertain whether AD-associated features can be reproduced in non-human primates upon brain administration of synthetic A $\beta$ O s.

Here, we show that the repeated A $\beta$ O injections into the cerebral parenchyma rapidly caused massive A $\beta$  plaques, evident neurofibrillary tangles, profound neuroinflammation, as well as selective neurodegeneration in adult cynomolgus monkeys, indicating that the progression of AD, at least the classical neuropathological features of patient at early phase, were reproduced in non-human primates. Moreover, our evidence implicated the correlation between the A $\beta$ O-stimulated A $\beta$  plaque development and subsequent tau tangle formation in cynomolgus brain. These results suggested that A $\beta$ O-monkeys could serve as a promising research model for uncovering the pathogenetic events of AD.

## RESULTS

### Massive A $\beta$ plaques developed in brain of A $\beta$ O-induced cynomolgus monkeys as in patients with AD

To determine whether the synthetic A $\beta$  oligomers (A $\beta$ O s) could induce pathological features associated with AD in non-human primates, we recruited 14 adult cynomolgus monkeys (7 in experimental group and 7 in control group) that were around 20 years old from the same colony (Table S1). Instead of lateral ventricle as previously reported (Fornly-Germano et al., 2014), we developed a new injection assay and bilaterally delivered soluble A $\beta$ O s to cerebral parenchyma, the white matter region adjacent to the dorsal and lateral hippocampus of cynomolgus monkeys. A total of 800  $\mu$ g A $\beta$ O s were delivered into each cynomolgus brain via four injections over 5 months (Figure 1A). The oligomerization of commercially synthetic human A $\beta$ <sub>1-42</sub> peptides was performed before each injection, and the freshly prepared A $\beta$ O s were analyzed by western blotting before and after each injection. The blotting data revealed that A $\beta$ <sub>1-42</sub> peptides consistently polymerized into soluble, low-molecular-weight oligomeric forms, mainly including dimers (~8 kDa), trimers (~12 kDa), and tetramers (~16 kDa) (Figure 1B), which are among the most neurotoxic A $\beta$ O species detected in the cerebrospinal fluid from patients with AD (McLean et al., 1999; Shankar et al., 2008). The dot blot by using both A $\beta$  oligomeric and fibrillary antibodies revealed that these low-molecular-weight assemblies of A $\beta$ <sub>1-42</sub> were soluble fibrillar oligomers (Figure 1C). Magnetic resonance imaging (MRI) scanning showed that the synthetic A $\beta$ O s were successfully delivered to the targeted parenchymal sites (Figure S1A).

As soon as 8 months after the fourth A $\beta$ O s injection, we started to examine the neuropathological features of AD in A $\beta$ O-induced cynomolgus brains. Immunohistochemistry with 6E10 was performed to detect possible amyloid deposits on brain sections from all 14 cynomolgus monkeys. To cover as many brain regions as AD affected, at least four serial sections from the anterior to posterior of each cynomolgus cerebrum were examined (Figure S1B). We screened the whole brain sections and found that A $\beta$  plaques intensely and specifically labeled by 6E10 spread to fill much of the striatum and prefrontal cortex (PFC) (Figures 1D and S1C); the frontal cortex (FC), striatum, temporal cortex (TC), and parietal cortex (PC) (Figures 1E and S1D); the PC, hippocampus (HPC), entorhinal cortex (EC), and TC (Figures 1F and S1E); and the PC, HPC, and TC (Figures 1G and S1F). In general, the A $\beta$  plaques were mainly distributed in gray matter regions of limbic structures and association cortex of cynomolgus monkeys as in patients. Most plaques were compact with a dense core or were small and partially compact, similar to the typical senile plaques in the cortex of patients with AD (Figures 1D–1G and S1C–S1F). The diffuse plaques and finely granular deposits were also observed in numerous brain regions (Figures 1D and 1E). The density of A $\beta$  plaques was distinct from brain region to region and also from monkey to monkey, but all seven A $\beta$ O-monkeys exhibited similar spatial patterns of amyloid deposition throughout the brain (Figures 1D–1G and S1C–S1F). In contrast, the brain sections from seven control cynomolgus monkeys remained relatively free of A $\beta$  plaques

Sciences, Guangzhou, 510530, China

<sup>10</sup>Institute for Stem Cell and Regeneration, Chinese Academy of Sciences, Beijing, 100101, China

<sup>11</sup>These authors contributed equally

<sup>12</sup>Lead contact

\*Correspondence:

fyuee@hotmail.com (F.Y.),  
cmjue@sibcb.ac.cn (C.Y.),  
njing@sibcb.ac.cn (N.J.)

<https://doi.org/10.1016/j.isci.2021.103207>

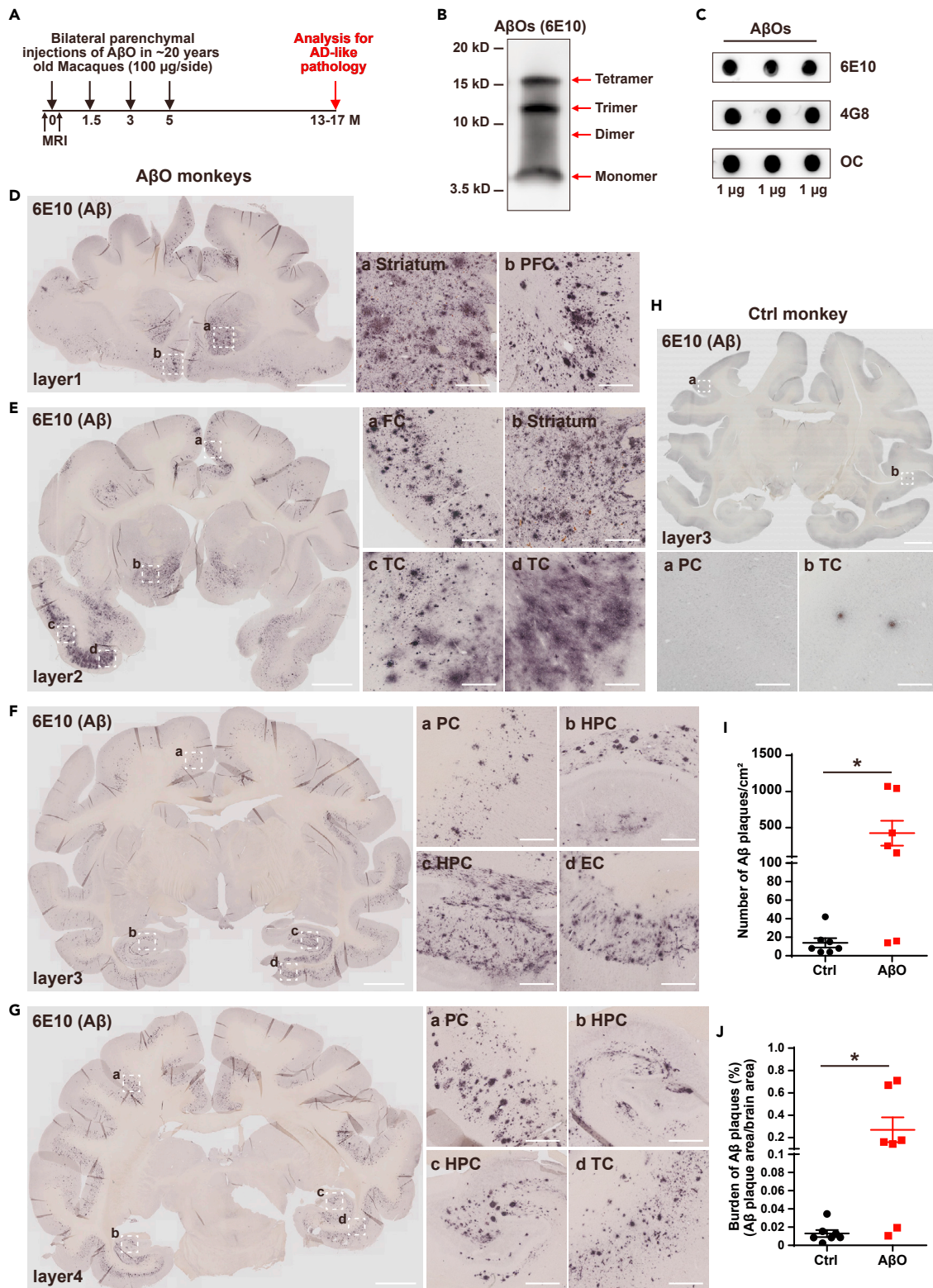


**Figure 1. The development of A $\beta$  plaques in A $\beta$ O-monkeys**

(A) Schematic diagram of delivering A $\beta$ O<sub>s</sub> into the parenchyma of cynomolgus monkeys (n = 7).

(B) Western blot analysis of synthetic A $\beta$ O<sub>s</sub> with the monoclonal antibody 6E10 immediately prior to each injection.

**Figure 1. Continued**

(C) Dot blot analysis of synthetic A $\beta$ O<sub>2</sub>s with A $\beta$  oligomeric and fibrillary antibodies 6E10, 4G8, and OC.

(D–G) Immunohistochemical analysis with 6E10 for detecting A $\beta$  plaques in brain sections from anterior to posterior cerebrum of A $\beta$ O<sub>2</sub>-monkeys and representative whole brain sections containing striatum and prefrontal cortex (D); frontal cortex, striatum, and temporal cortex (E); parietal cortex, hippocampus, and entorhinal cortex (F); and parietal cortex, hippocampus, and temporal cortex (G). In the right panel, enlarged views of the outlined regions clearly indicate the massive A $\beta$  plaques in different brain regions.

(H) Immunohistochemical analysis with 6E10 for detecting A $\beta$  plaques in representative whole brain section from cerebrum of the control monkey. In the bottom panel, enlarged views of the outlined regions indicate that A $\beta$  plaques are absent or very sparse in different brain regions.

(I) Quantification analysis of the numbers of A $\beta$  plaques in the cerebrum of control (n = 7) and A $\beta$ O<sub>2</sub>- (n = 7) cynomolgus monkeys (p = 0.0345).

(J) Quantification analysis of the burden of A $\beta$  plaques in the cerebrum of control (n = 7) and A $\beta$ O<sub>2</sub>- (n = 7) monkeys (p = 0.0394). Data are represented as mean  $\pm$  SEM. Each symbol represents an individual cynomolgus monkey. Statistical differences are evaluated with two-tailed unpaired Student's t test. \*p < 0.05. Scale bars: 5 mm (whole brain images in C–G), 200  $\mu$ m (enlarged views in C–G). Abbreviations: PFC, prefrontal cortex; FC, frontal cortex; TC, temporal cortex; PC, parietal cortex; HPC, hippocampus; and EC, entorhinal cortex. See also [Figure S1](#) and [Table S1](#).

or occasionally harbored a few distributing in some limited brain regions, such as TC ([Figure 1H](#)). We counted the A $\beta$  plaques and found that three of the seven A $\beta$ O<sub>2</sub>-monkeys displayed massive and highly clustered A $\beta$  plaques ([Figures 1D–1G](#)), two contained moderate numbers of A $\beta$  plaques ([Figures S1C–S1F](#)), and the rest two had a few plaques. The number and burden of A $\beta$  plaques in seven A $\beta$ O<sub>2</sub>-monkeys were apparently higher than those in seven control monkeys, indicating that synthetic A $\beta$ O<sub>2</sub>s can efficiently drive A $\beta$  deposition in the brain of cynomolgus monkeys ([Figures 1I](#) and [1J](#)).

To confirm the formation of AD-like A $\beta$  plaques in A $\beta$ O<sub>2</sub>-monkeys, the A $\beta$  plaques in monkey brain were carefully characterized by different measurements. The immunostaining with the most frequently used A $\beta$  plaque-specific antibodies, 6E10 and 4G8, revealed multiple plaque subtypes in A $\beta$ O<sub>2</sub>-monkeys as in patients with AD, such as compact plaques mostly having clear-cut outlines ([Figures 2A–2D](#), left panels), cotton-wool plaques ([Figure 2A](#), right panel), cored plaques with miliary focus ([Figure 2C](#), right panel), as well as diffuse plaques usually displaying ill-defined surfaces and flake-like deposits ([Figures 2B](#) and [2D](#), right panels), indicating that A $\beta$  plaques in the cortex of A $\beta$ O<sub>2</sub>-monkeys morphologically and immunoreactively resembled those in patients with AD. In addition, the A $\beta$  plaques in A $\beta$ O<sub>2</sub>-monkey brain were recognizable by other standard measurements that are usually performed to detect A $\beta$  plaques in the patient brain, including silver ([Figure 2E](#)), Thioflavin S ([Figure 2F](#)), and Congo Red staining ([Figure 2G](#)). Aligned with the immunostaining results, the western blot with 6E10 detected A $\beta$ -positive bands in FC and TC of A $\beta$ O<sub>2</sub>-monkeys, which was similar to the band from 5XFAD mouse brain with A $\beta$  plaques ([Figure 2H](#)). There was no detectable A $\beta$ -band from brain tissues of control monkeys ([Figure 2H](#)), which was consistent with the previous findings ([Oikawa et al., 2010](#)). The cynomolgus monkeys were proven to display age-related increases in A $\beta$  plaques. Yet in brains of cynomolgus monkeys around 20 years old, the A $\beta$  plaques were absent by western blot analysis or unfrequently detected in limited brain regions by immunohistochemistry ([Oikawa et al., 2010](#)). Together, A $\beta$  plaques quickly developed in the cortex of cynomolgus monkeys upon A $\beta$ O<sub>2</sub> administration, which was similar to the A $\beta$  deposits abundantly present in patients with AD and indicative of the amyloid pathology in the A $\beta$ O<sub>2</sub>-monkeys.

**Overt neurofibrillary tangles formed in multiple brain regions of A $\beta$ O<sub>2</sub>-induced cynomolgus monkeys**

Microtubule-associated protein tau is abnormally phosphorylated in AD brain and aggregates as paired helical filaments (PHFs) in neurofibrillary tangles that is another hallmark of AD ([Lee et al., 2001](#)). Then, we detected whether A $\beta$ O<sub>2</sub>-monkeys captured neurofibrillary tangles or dystrophic neurites in the brain. Similar to what was performed for the measurements of A $\beta$  plaques, serial sections from anterior to posterior cynomolgus cerebrum were recruited and examined by different hyperphosphorylated tau antibodies against PHFs. Since the various transgenic mice that have been widely used failed to develop tauopathy, it was exciting to observe neurofibrillary tangles reactive with AT8 ([Figure 3](#)) and AT100 ([Figure S2](#)) in multiple brain regions of A $\beta$ O<sub>2</sub>-monkeys, such as PFC, PC, TC, EC, striatum, HPC, thalamus, and medium septum. The developed neurofibrillary tangles in A $\beta$ O<sub>2</sub>-monkeys were confirmed by a silver-based histological method that was routinely used to visualize tau tangles in patients with AD ([Figure S3](#)). The filamentous aggregations with densely immunoreactive signals were generally detected in the cell soma (arrows) or the long axons (arrowheads) and outstretched dendrites, which were morphologically reminiscent of those in the brain of patients with AD ([Figures 3](#) and [S2](#)). Apparently, the neurofibrillary tangles consisting of PHF in A $\beta$ O<sub>2</sub>-monkeys were mostly intracellular. The accumulation of AT8<sup>+</sup> PHF was detected in the cytoplasm of either NF-H<sup>+</sup> neurons ([Figures 3A–3C](#)) or GFAP<sup>+</sup> astrocytes ([Figures 3D](#) and [3E](#)).

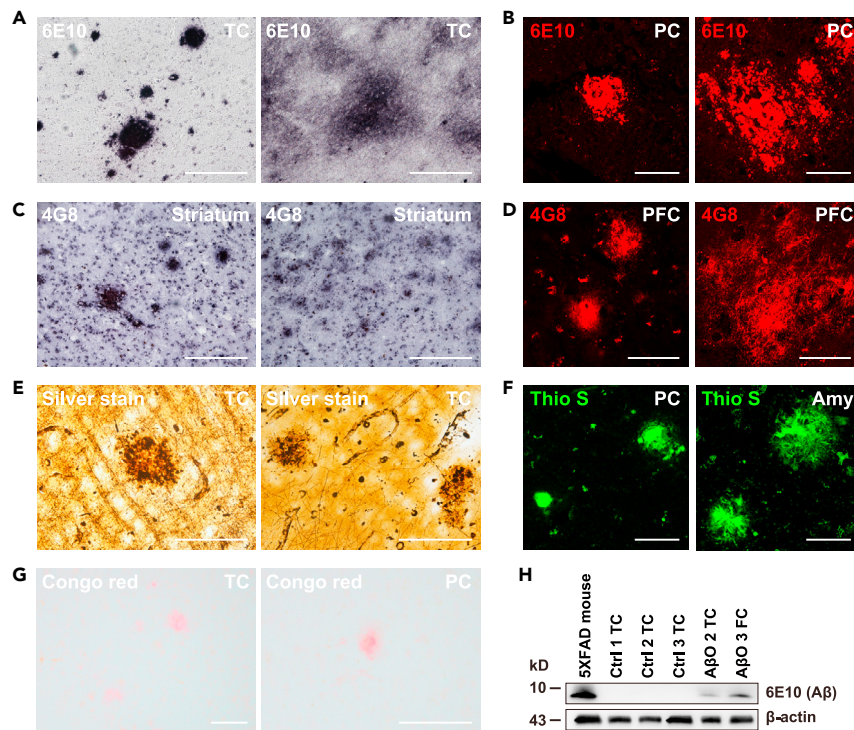


**Figure 2. The characterization of developed Aβ plaques in AβO-monkeys**

(A and B) The representative subtypes of Aβ plaques detected by immunohistochemical (A) and immunofluorescent (B) analysis with 6E10.  
 (C and D) The representative subtypes of Aβ plaques detected by immunohistochemical (C) and immunofluorescent (D) analysis with 4G8.  
 (E) The histological visualization of Aβ plaques in the brain of AβO-monkeys by a silver-based staining method similar to that used by Alois Alzheimer to detect tangles in his index case.  
 (F) The detection of Aβ plaques by Thioflavin S staining.  
 (G) The detection of Aβ plaques by Congo red staining.  
 (H) Western blot analysis of tissue homogenates from different brain regions, including cortex of a 5XFAD mouse with massive Aβ plaques as the positive control, temporal cortex of control monkeys #1, #2, #3 and AβO-monkey #2, and frontal cortex of AβO-monkey #3 with 6E10, and β-actin was used as a loading control. Scale bars: 200 μm (A and C), 100 μm (E and G), and 50 μm (B, D, and F). Abbreviations: TC, temporal cortex; PC, parietal cortex; Amy, amygdala; PFC, prefrontal cortex.

The general shape of tangle-bearing neurons or astrocytes appeared normal (Figures 3 and S2), exhibiting detectable nucleus (Figures 3C and 3E). The more detailed characterization revealed that the neurofibrillary tangles in AβO-monkeys developed typical structures as those in patients with AD, such as bundles of convoluted filaments in the cell soma (Figure 4A, arrows) or droplet-like inclusions appearing like a string of pearls in long axons (Figures 4A and 4B, solid arrowheads). Some neurons displayed nonfibrillar punctate regions in the cytoplasm with diffuse staining, the typical features of pre-tangle state in the brain of patients with AD (Figures 4A and 4B, stars). Neuropil threads with breakdown of dendritic and axonal structures were found in multiple brain regions, such as hippocampus and PC (Figures 4A and 4B, empty arrowheads). Therefore, the neurofibrillary tangles in AβO-monkeys acquired the features of typical tangles described in patients with AD (Augustinack et al., 2002). The classic neuritic plaques are defined as combined deposits consisting of insoluble Aβ with dystrophic neurites that contain aggregated tau, which develop only in the late phase of the disease process (Braak and Del Tredici, 2015). Some Aβ plaques in the brain of AβO-monkeys occurred with AT8<sup>+</sup> dystrophic neurites (Figure 4C). These plaques displayed amyloid cores and surrounded neurites, resembling the neuritic plaques in patients with AD.

It is noteworthy that the naturally occurring human-like neurofibrillary tangles with PHF have never been definitively identified in aged primate species, even in those with advanced Aβ deposition (Härtig et al., 2000;

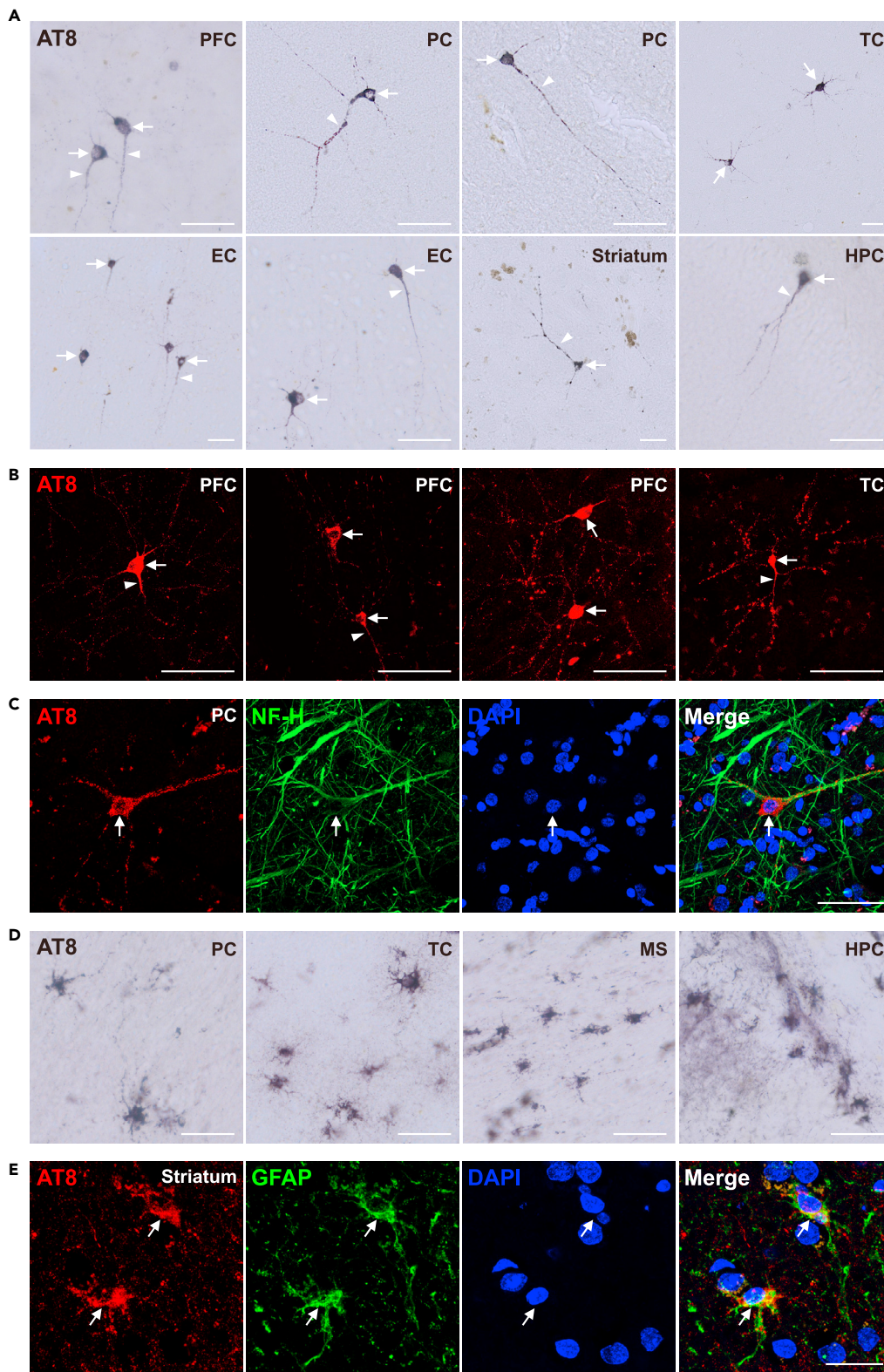


**Figure 3. The formation of neurofibrillary tangles (NFTs) in A $\beta$ O-monkeys**

(A and B) Immunostaining analysis for detecting NFTs from anterior to posterior brain sections of A $\beta$ O-monkeys and representative brain regions containing AT8-positive tau tangles in neurons (immunohistochemical images in A and immunofluorescent images in B). The arrows indicate NFTs in soma bodies, and arrowheads indicate long axons with droplet-like staining.

(C) The double immunostaining with AT8 and neuronal antibody NF-H.

(D) Immunohistochemical analysis for detecting NFTs from anterior to posterior brain sections of A $\beta$ O-monkeys and representative brain regions containing AT8-positive tau tangles in astrocytes.

(E) The double immunostaining with AT8 and astrocyte antibody GFAP. Scale bars: 100  $\mu$ m (B), 50  $\mu$ m (A, C, and D), and 25  $\mu$ m (E). Abbreviations: PFC, prefrontal cortex; PC, parietal cortex; TC, temporal cortex; EC, entorhinal cortex; HPC, hippocampus; MS, medium septum. See also [Figures S2](#) and [S3](#).

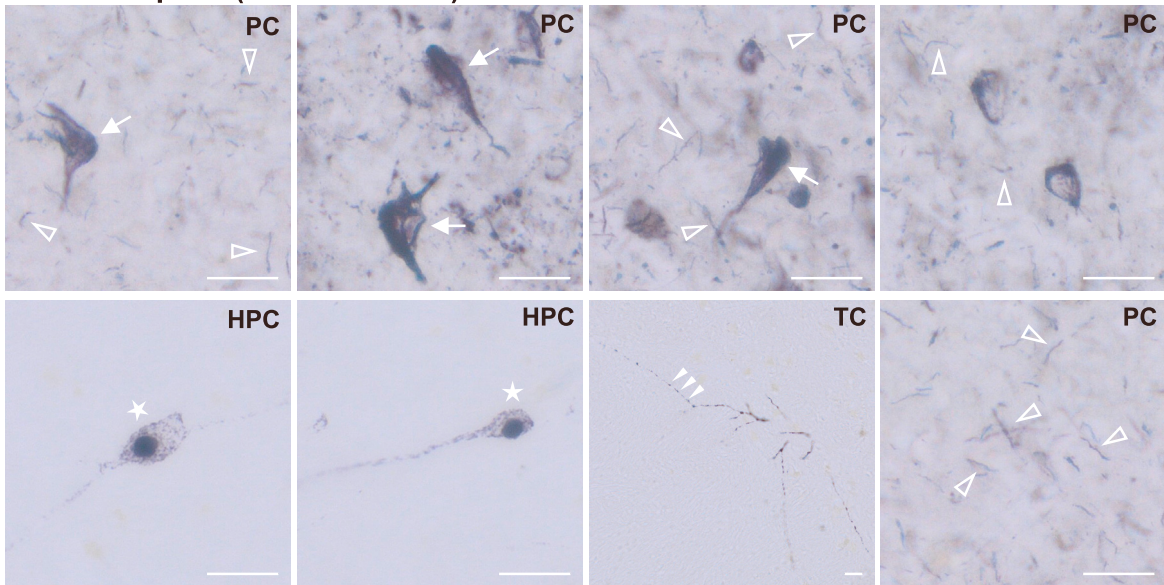
[Oikawa et al., 2010](#)). The only exception is a 41-year-old chimpanzee that had a left hemisphere stroke, which displayed human-like tau tangles but without the typical AD distribution ([Rosen et al., 2008](#)). Consistent with the paucity of neurofibrillary tangles in aged cynomolgus macaque, we did not detect any tau tangles or abnormally phosphorylated tau in the seven control monkeys ([Table 1](#)). In general, A $\beta$ O-induced neurofibrillary tangles in cynomolgus brain were scattered and not as massive as A $\beta$  plaques. The neurofibrillary tangles were observed in six of the seven A $\beta$ O-monkeys, showing an apparent correlation between the formation of tau lesions and A $\beta$  plaques ([Table 1](#)). The soluble A $\beta$ O caused two classical AD signatures in the brain of monkeys, arguing in favor of the amyloid-cascade hypothesis for human AD. Together, we detected the formation of intracellular neurofibrillary tangles that are strikingly reminiscent of tauopathy in patients with AD and, therefore, identified a co-occurrence of amyloid and tau pathology in A $\beta$ O-monkeys.

**Pronounced neuroinflammation was triggered in the brain of A $\beta$ O-induced cynomolgus monkeys**

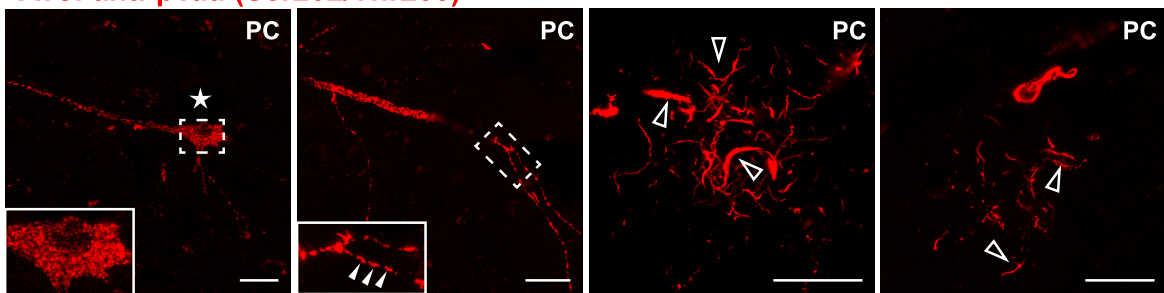
In addition to A $\beta$  plaques and tau pathology, neuroinflammation is another key neuropathological feature of AD and is characterized by the presence of activated astrocytes and microglia surrounding A $\beta$  plaques ([Wyss-Coray and Mucke, 2002](#)). Immunostaining analysis revealed that the GFAP<sup>+</sup> astrocytes preferred to accumulate in the white matter region of cortex from both control and A $\beta$ O-monkeys ([Figure 5A](#)). The activated astrocytes exhibiting much larger soma and a more complex morphology were often found in the cortex of A $\beta$ O-cynomolgus brains ([Figures 5A](#) and [5B](#)). The total number of astrocytes in brain regions measured was much higher in A $\beta$ O-monkeys than in controls ([Figure 5C](#)). Some activated astrocytes were detected to surround A $\beta$  plaques in some brain regions of A $\beta$ O-monkeys, such as PFC and PC ([Figure 5D](#)). In general, the spatial distribution of Iba1<sup>+</sup> microglia spread over the entire cortex of monkey and an abundant of microglia were observed in the gray matter regions of the A $\beta$ O-monkeys ([Figure 5E](#)), which was distinct from that of the astrocytes ([Figures 5A](#) and [5B](#)). The activated microglia with larger soma and more complex morphology showed an increased tendency in some brain regions of A $\beta$ O-monkeys ([Figures 5F](#) and [5G](#)). Quite a number of activated microglia surrounded A $\beta$  plaques and drove the neuroinflammation in multiple brain regions of A $\beta$ O-monkeys, such as PFC, EC, PC, and HPC ([Figure 5H](#)). This was distinct from that observed in the brains of the control monkeys ([Figure S4](#)). Compared with the astrocytes, more microglia were activated by and situated within or near the core of A $\beta$  plaques in A $\beta$ O-monkeys. The activated microglia and astrocytes intimately surrounding or within A $\beta$  plaques in A $\beta$ O-monkeys were in line with the observations in the brain of patients with AD. These results indicated that neuroinflammation was triggered in the cynomolgus brain upon A $\beta$ O treatment.

Since the key pathological features as occurring at the early phase of AD were detected in the cynomolgus brain upon the administration of synthetic A $\beta$ O, we next sought to investigate the intervening steps among them. Recent studies have shown that A $\beta$ -activated inflammasome in microglia, the central signaling hubs of neuroinflammatory processes, play fundamental roles in the initiation and progression of AD ([Kelley et al., 2019](#); [Lucin and Wyss-Coray, 2009](#); [Meyer-Luehmann et al., 2008](#); [Weiner and Frenkel, 2006](#)). The activation of inflammasomes, which is marked by the formation of ASC specks and the increase of cleaved caspases-1, was detected in the cortex of patients with AD ([Franklin et al., 2018](#); [Heneka et al., 2013](#)). In the cortex of A $\beta$ O-monkeys, we found extracellular ASC specks surrounding A $\beta$  plaques or adjacent to tau tangles ([Figures S5A](#) and [S5B](#)). Moreover, the formation of ASC specks showed a correlation to the abundance of A $\beta$  plaques and tau tangles ([Table 1](#)). In contrast, the ASC specks were seldom observed in control monkeys, except a few around A $\beta$  plaques in two control brains ([Figures S5A](#) and [S5B](#); [Table 1](#)). Consistently, we detected increased level of cleaved caspase-1 in some brain regions of A $\beta$ O-monkeys, as

**A AT8: anti-pTau (Ser202/Thr205)**



**B AT8: anti-pTau (Ser202/Thr205)**



**C**

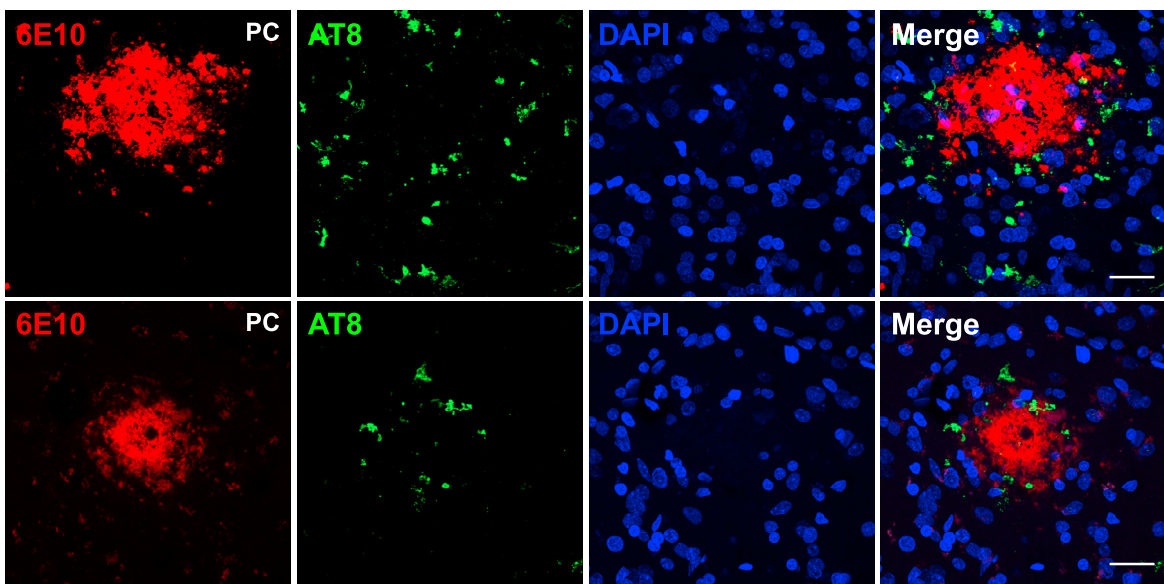


**Figure 4. The characterization of developed NFTs in AβO-monkeys**

(A and B) The representative forms of NFTs detected by immunohistochemical (A) and immunofluorescent (B) analysis with AT8. The arrows indicate the NFTs in cell soma, empty arrowheads indicate neuropil threads, solid arrowheads indicate droplet-like inclusions in long axons, and stars indicate nonfibrillar punctate staining in pre-tangles.

(C) The double immunostaining with 6E10 and AT8 for the detection of neuritic plaques. Scale bars: 100 μm (B), 50 μm (A, C). Abbreviations: PC, parietal cortex; HPC, hippocampus; TC, temporal cortex.

in the cortex of patients with AD (Figures S5C and S5D). These observations indicated that the inflammasome/caspase-1 signal was activated in AβO-monkeys as in patients with AD, suggesting a role of inflammasome in the AβO-driven Aβ plaques and tau tangles formation.

**Selective neurodegeneration was detected in multiple brain regions of AβO-induced cynomolgus monkeys**

In patients with AD, the early pathological changes, including Aβ plaques, tau tangles, and neuroinflammation, ultimately lead to neural degeneration and neuron loss, which are hallmark events occurring at the later phase of AD. Fluoro-Jade C (FJC) is a fluorochrome that has been widely used to detect neuronal neurodegeneration (Schmued et al., 1997). We found the FJC-positive neurons in different brain regions of AβO-monkeys, such as PFC, PC, and TC (Figure 6A). The FJC<sup>+</sup> neurons were always in close physical contact with Aβ plaques, indicative of the selective neural degeneration in the AβO-cynomolgus brain (Figure 6A). The nuclear staining of FJC<sup>+</sup> neurons was less intensive than that of FJC<sup>-</sup> cells around, and some even disappeared in neurons with much stronger FJC signals (Figure 6A, arrows). Consistently, the density of immunoreactive signals in the nucleus of NEUN<sup>+</sup> neurons bearing AT8<sup>+</sup> tangles was much weaker than in neurons without tangles (Figure 6B). The expression of necroptosis cell death marker, pMLKL, was detected around or in the nucleus of some neural cells in AβO-cynomolgus brain (Figure S6), which is consistent with the measurements of pMLKL in patients with AD (Caccamo et al., 2017; Koper et al., 2020). Referring to the degeneration or loss of synapses due to AβO treatment, we found that the decline of density and intensity of Synaptophysin<sup>+</sup> dots in the brain of AβO-monkeys was profound compared to those in control brain (Figures 6C, 6D, and S7). We also examined the possible neuron loss in specific brain regions of AβO-monkeys. Compared with control monkeys, the numbers of ChAT<sup>+</sup> basal forebrain cholinergic neurons of AβO-monkeys were low but not significantly lower (Figures 6E and 6F). Thus, the AβO-monkeys exhibited selective neurodegeneration that appeared to correlate with Aβ plaques but did not display obvious neuron loss yet.

**Table 1. The occurrence of amyloid and tau pathology, as well as inflammasome activation in the brain of AβO-induced cynomolgus monkeys**

| Monkey number | Ab plaque number/cm <sup>2</sup> | Ab plaque area/brain area (%) | Tau tangles | ASC specks/Aβ plaque | ASC specks adjacent to tau tangle |
|---------------|----------------------------------|-------------------------------|-------------|----------------------|-----------------------------------|
| AβO-1         | 1,071                            | 0.7103                        | +           | ++                   | +                                 |
| AβO-2         | 1,042                            | 0.6686                        | ++          | ++                   | +                                 |
| AβO-3         | 426                              | 0.1616                        | +++         | +++                  | +                                 |
| AβO-4         | 250                              | 0.1772                        | +           | +                    | +                                 |
| AβO-5         | 149                              | 0.1439                        | +           | +                    | ++                                |
| AβO-6         | 16                               | 0.0193                        | ND          | -                    | -                                 |
| AβO-7         | 14                               | 0.0106                        | +           | +                    | -                                 |
| Ctrl-1        | 15                               | 0.013                         | ND          | +                    | -                                 |
| Ctrl-2        | 8                                | 0.0086                        | ND          | -                    | -                                 |
| Ctrl-3        | 17                               | 0.0088                        | ND          | -                    | -                                 |
| Ctrl-4        | 4                                | 0.0025                        | ND          | -                    | -                                 |
| Ctrl-5        | 4                                | 0.0085                        | ND          | -                    | -                                 |
| Ctrl-6        | 42                               | 0.0345                        | ND          | +                    | -                                 |
| Ctrl-7        | 8                                | 0.0154                        | ND          | +                    | -                                 |

Footnotes: +++, high; ++, medium; +, low; -, absence; N.D., not detected.

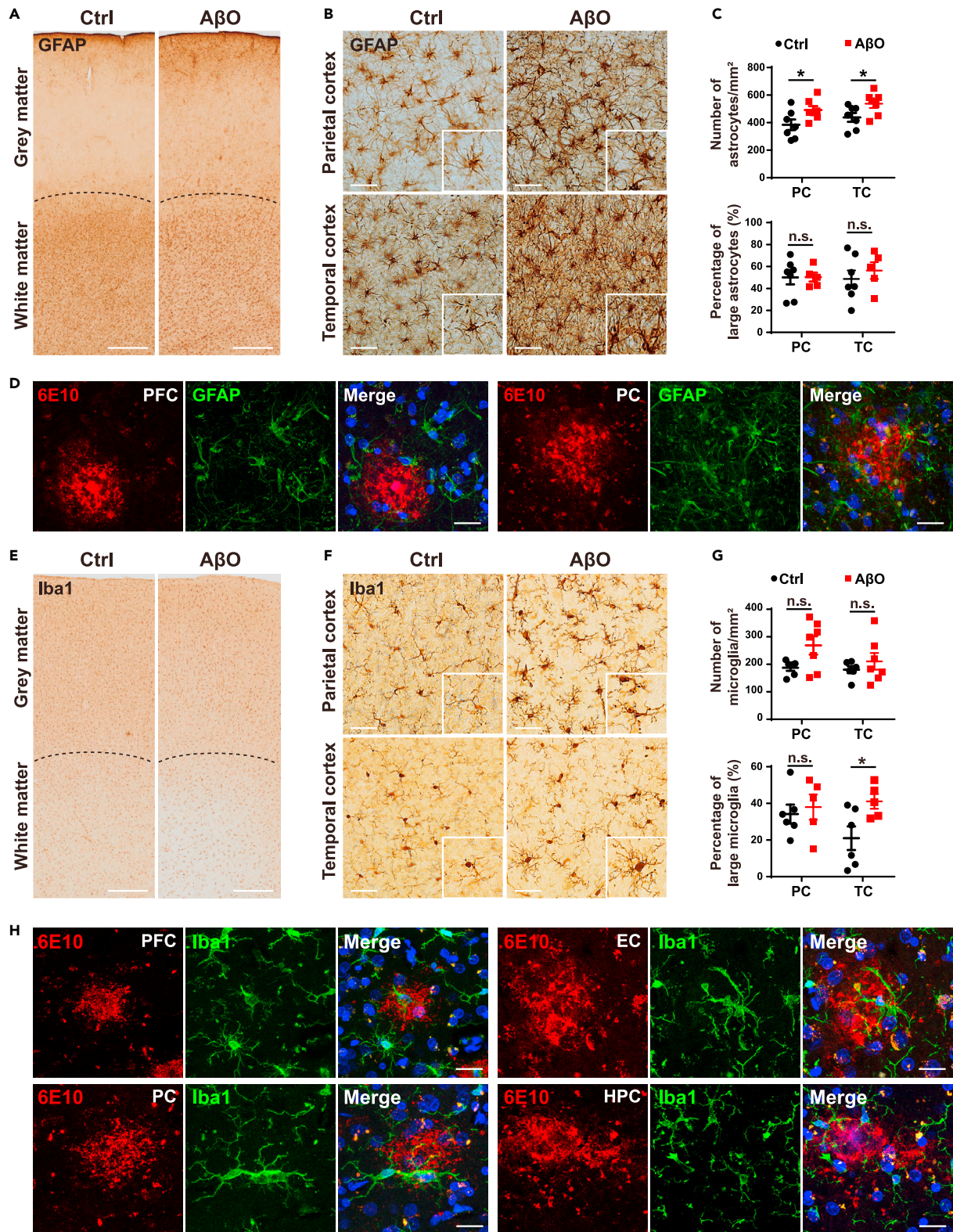


**Figure 5. The activated astrocytes and microglia in A $\beta$ O-monkeys**

(A) Immunohistochemical analysis with GFAP antibody to detect astrocytes in the cortex of cynomolgus monkeys.  
(B) The GFAP<sup>+</sup> astrocytes in different brain regions of control or A $\beta$ O-monkeys. The close-up views show the larger soma and a more complex morphology of activated astrocytes in A $\beta$ O-monkeys.  
(C) Quantification analysis of the density of total astrocytes in PC ( $p = 0.0436$ ) and TC ( $p = 0.0455$ ) and percentage of activated astrocytes in PC ( $p = 0.7625$ ) and TC ( $p = 0.8554$ ) of control ( $n = 7$ ) and A $\beta$ O- ( $n = 7$ ) monkeys.  
(D) Double immunofluorescence staining analysis to detect A $\beta$  plaques and activated astrocytes in different brain regions of A $\beta$ O-monkeys. Note that some activated astrocytes are associated with A $\beta$  plaques.  
(E) Immunohistochemical analysis with Iba1 antibody to detect microglia in the cortex of cynomolgus monkeys.  
(F) The Iba1<sup>+</sup> microglia in different brain regions of control and A $\beta$ O-monkeys. The close-up views show the larger soma and a more complex morphology of activated microglia in A $\beta$ O-monkeys.  
(G) Quantification analysis of the density of total microglia in PC ( $p = 0.0531$ ) and TC ( $p = 0.4057$ ) and percentage of activated microglia in PC ( $p = 0.4798$ ) and TC ( $p = 0.1408$ ) of control ( $n = 7$ ) and A $\beta$ O- ( $n = 7$ ) monkeys.  
(H) Double immunofluorescence staining analysis to detect A $\beta$  plaques and activated microglia in different brain regions of A $\beta$ O-monkeys. Note that some activated microglia are associated with A $\beta$  plaques. Data are represented as mean  $\pm$  SEM. Each symbol represents an individual cynomolgus monkey. Statistical differences are evaluated with two-tailed unpaired Student's *t* test. n.s., no significant difference. \* $p < 0.05$ . Abbreviations: PFC, prefrontal cortex; PC, parietal cortex; TC, temporal cortex; EC, entorhinal cortex; HPC, hippocampus. Scale bars: 500  $\mu$ m (A and E), 50  $\mu$ m (B and F), and 25  $\mu$ m (D and H). See also [Figures S4](#) and [S5](#).

**Delivering A $\beta$ O into cerebral parenchyma induces AD-like pathological features**

Previous studies usually delivered the soluble A $\beta$ O into the lateral ventricles of non-human primates, such as marmosets or rhesus monkeys ([Baker et al., 1993](#); [Geula et al., 1998](#)), which was different from the intraparenchymal injections of A $\beta$ O in the current study. Thus, six more adult cynomolgus monkeys were recruited to test the reliability of the parenchyma-based approach ([Table S2](#)). Three monkeys received A $\beta$ O through parenchyma same as the previous seven monkeys, the other three through lateral ventricles as previously reported ([Figures 7A](#) and [7B](#)). Compared with the first experiment, we increased the dosage and injection times of A $\beta$ O for each monkey ([Figures 7A](#) and [7B](#)). We detected strong A $\beta$  deposition in global brains of two intraparenchymal monkeys 5 months after the last injection ([Figures 7C](#), [7E](#), and [S8A](#); [Table S2](#)) and very few A $\beta$  plaques in limited brain regions of one intracerebroventricular monkey ([Figures 7D](#), [7F](#), and [S8B](#); [Table S2](#)). More interestingly, only the two intraparenchymal monkeys with intensive A $\beta$  plaques displayed obvious neurofibrillary tangles ([Figures 7G](#) and [7I](#); [Table S2](#)). Therefore, the intraparenchymal delivery stimulated AD-like conditions in these two adult cynomolgus monkeys. Finally, we detected the activated astrocytes and microglia in the monkey brains ([Figures S8C](#) and [S8D](#)). Together, we advanced the approach by delivering the synthetic A $\beta$ O into parenchyma of cynomolgus brain and reliably reproduced the pathologic phenotypes of early AD in non-human primates.

**DISCUSSION**

In this study, we systematically elucidated that the adult cynomolgus monkeys rapidly captured most of key features of early AD, such as extracellular A $\beta$  plaques, intracellular tau tangles, neuroinflammation, and selective neurodegeneration upon the repeated intraparenchymal delivery of synthetic A $\beta$ O. The A $\beta$ O-monkeys rapidly and fully developed the early neuropathological features of AD.

A $\beta$  deposition and neurofibrillary tangles are the central events during the early pathogenesis of AD. In a Matrigel-based 3D-culture system, expressing amyloid  $\beta$  precursor protein (APP) and presenilin 1 (PS1) with familial AD mutations in human neural progenitor cells induced extracellular A $\beta$  deposition and filamentous tau ([Choi et al., 2014](#); [Kwak et al., 2020](#)). However, the established AD animals usually display A $\beta$  plaques in the absence of tau tangles. Neither the traditional AD mouse nor newly reported human-mouse chimeric AD model reproduced tangle pathology ([Espuny-Camacho et al., 2017](#)). The critical discrepancy existing in currently available AD model animals has hampered the understanding of molecular biology, biochemistry, and neuropharmacology of AD ([LaFerla and Green, 2012](#)). In this study, we found that the repeated parenchymal injections of synthetic A $\beta$ O induced massive A $\beta$  plaques in the entire brain of adult cynomolgus monkeys ([Figures 1](#), [2](#), [7](#), [S1](#), and [S8](#)). In addition, eight monkeys with extensive A $\beta$  plaques from two independent experiments displayed neurofibrillary tangles and neuropil threads in multiple brain regions as well as neuritic plaques with A $\beta$  aggregation and dystrophic neurites. These observations revealed the formation of tau tangles in monkeys and also demonstrated that the formation of tau tangles is well correlated with the development of A $\beta$  plaques in cynomolgus brain ([Figures 3](#), [4](#), and [7](#); [Table 1](#)). The acute treatment (weeks) by delivering soluble A $\beta$ O into the lateral ventricles could not induce the co-occurrence of A $\beta$  plaques and tau tangles in cynomolgus monkeys in previous studies ([Forny-Germano](#)

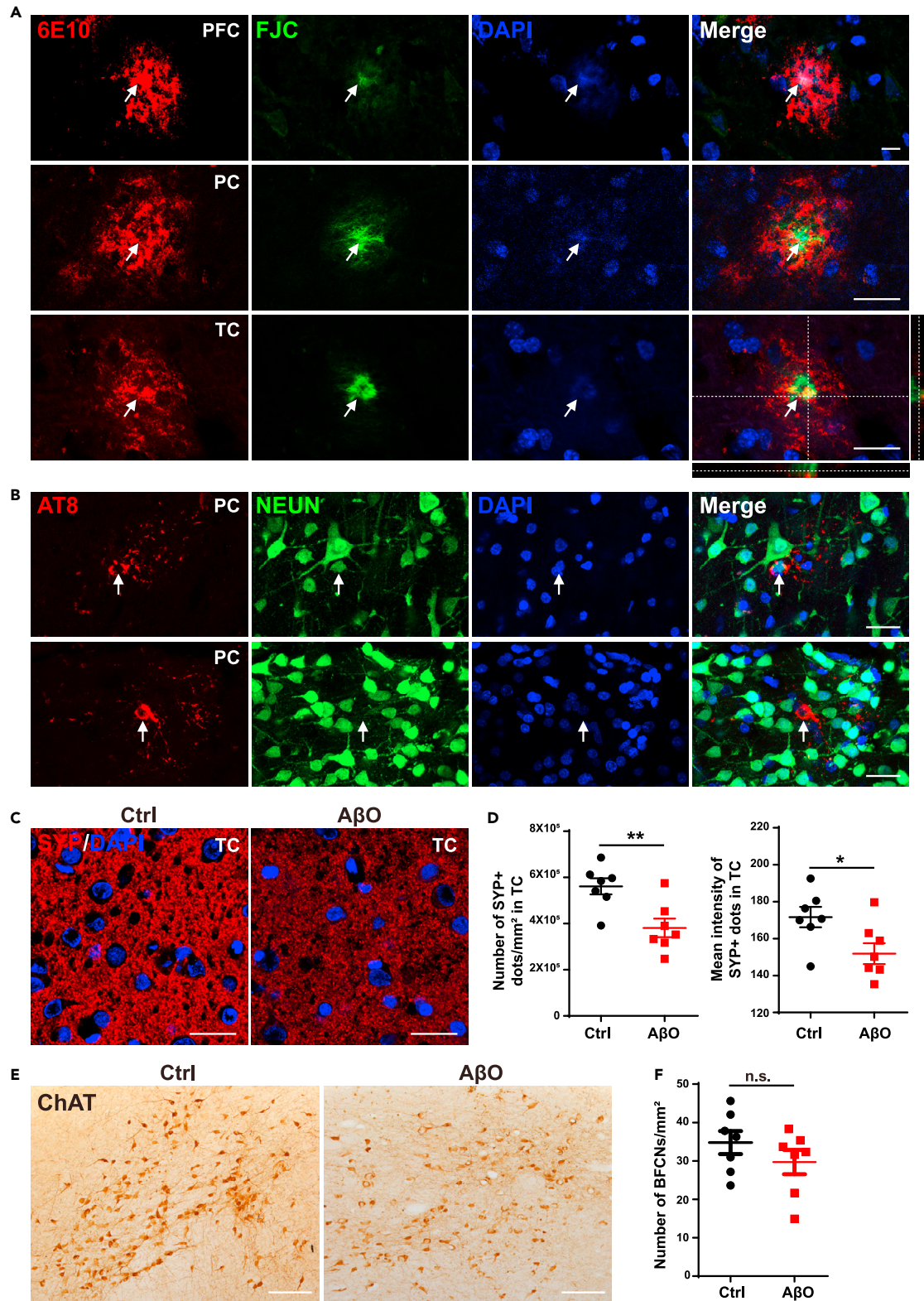


**Figure 6. The neurodegeneration in AβO-monkeys**

(A) The degenerative neurons visualized by Fluoro-Jade C (FJC) were physically associated with 6E10-positive Aβ plaques in different brain regions of AβO-monkeys. Note the nucleus with faint signals in degenerative neurons.

**Figure 6. Continued**

(B) The detection of AT8<sup>+</sup> tangle-bearing neurons with degenerated nucleus.

(C) The immunofluorescence staining to detect the expression of presynaptic marker Synaptophysin (SYP) in the temporal cortex of control and A $\beta$ O-monkeys.

(D) Quantification analysis of the density ( $p = 0.0054$ ) and intensity ( $p = 0.0404$ ) of SYP<sup>+</sup> dots in the temporal cortex of control ( $n = 7$ ) and A $\beta$ O- ( $n = 7$ ) monkeys.

(E and F) ChAT-positive basal forebrain cholinergic neurons in basal forebrain (E) and corresponding quantification of control ( $n = 7$ ) and A $\beta$ O- ( $n = 7$ ) monkeys ( $p = 0.2651$ ) (F). Data are represented as mean  $\pm$  SEM. Each symbol represents an individual cynomolgus monkey. Statistical differences are

evaluated with two-tailed unpaired Student's *t* test. n.s., no significant difference. \* $p < 0.05$ , \*\* $p < 0.01$ . Abbreviations: PFC, prefrontal cortex; PC, parietal cortex; TC, temporal cortex. Scale bars: 25  $\mu$ m (A-C) and 200  $\mu$ m (E). See also [Figures S6](#) and [S7](#).

[et al., 2014](#)). Thus, it is exciting to find that two AD hallmarks, A $\beta$  plaques and tau tangles, were simultaneously reproduced in A $\beta$ O-monkeys. In the current study, the detected A $\beta$  plaques and tau tangles were carefully characterized by most frequently used antibodies and standard techniques. It is better to further confirm the conformation of tau tangles by other documented approaches, such as electron microscopy, which will be addressed in our future studies. In addition to A $\beta$  plaques and tau tangles, the A $\beta$ O-monkeys displayed activated astrocytes, microglia, and inflammasome associated with A $\beta$  plaques, which was indicative of the neuroinflammation in A $\beta$ O-monkeys ([Figures 5](#), [S4](#), and [S5](#)). Together, the key pathologic changes that are in the chain of events leading to AD developed in cynomolgus brain and the pathogenic process of early AD were recapitulated in monkeys upon administration of synthetic A $\beta$ O. In this regard, the central questions in AD pathogenesis, such as the nature of the pathologic relationship between A $\beta$  and tau, even the molecular and cellular alterations that precede A $\beta$  and tau lesions, could be interrogated over time in the A $\beta$ O-monkeys.

Being a unique human brain disorder, AD has not yet been discovered in other aged primates, no matter in captive or wild habitats ([Rosen et al., 2016](#); [Walker and Jucker, 2017](#)). These observations suggested that primate species might not be as predisposed to AD as humans, even though some aged primate species display numerous biological commonalities and substantial deposition of A $\beta$  in the brain ([Cramer et al., 2018](#); [Edler et al., 2017](#); [Oikawa et al., 2010](#); [Selkoe et al., 1987](#)). In this regard, to develop a genetically modified monkey model that can fully capture the complete spectrum of AD might be more challenging than previous anticipations. In addition, the performance of genetic modifications related to AD was more difficult in monkeys than in rodents, even with the recent advances in gene editing technologies. Furthermore, because of the slow and insidious process of AD and long lifespans of non-human primates, AD pathogenesis in genetically modified monkeys might require a long time to develop, years or even decades. In this study, cynomolgus monkeys with A $\beta$ O treatment rapidly displayed most neuropathologic changes of early AD within a year, which was even much faster than the generation of a transgenic AD mouse line with only one or two AD pathologic features. We further confirmed that delivering A $\beta$ O into parenchyma but not lateral ventricle drove the early AD-like conditions in cynomolgus monkeys. In two separate experiments and among all 10 adult cynomolgus monkeys, the parenchymal delivery of A $\beta$ O caused strong AD-like conditions in 8 adult cynomolgus monkeys, whereas the intracerebroventricular delivery of A $\beta$ O did not trigger dramatic neuropathological changes in the brain of rodents ([Malm et al., 2006](#)) and monkeys ([Forny-Germano et al., 2014](#)), which are in line with the observations shown in [Figure 7](#). The mechanism underlying remains unclear, but we deduced that the dosage, injection site, duration time, and injection frequency of A $\beta$ O would be key factors driving the pathological changes in monkey brain. Therefore, the repeated injections of A $\beta$ O into the parenchyma might be a reliable way to reproduce AD-like features in cynomolgus monkeys.

Mechanistically, a bunch of key questions still remain unsettled. The biggest one is how the synthetic A $\beta$ O instigated the buildup of A $\beta$  plaques and triggered the AD-like pathogenic cascade in cynomolgus brain. We wonder whether the synthetic A $\beta$ O directly aggregate into plaques or the synthetic A $\beta$ O stimulate the endogenous production of excessive A $\beta$ s to form A $\beta$  plaques or both contribute to the A $\beta$  plaque development in cynomolgus brain. Also, it is intriguing to know whether the synthetic A $\beta$ O directly initiated tau tangles, neuroinflammation, as well as neurodegeneration or the synthetic A $\beta$ O initiated amyloidopathy and thereby drove the subsequent pathogenic process in the cynomolgus monkeys. Evidences recently collected from different experimental systems show that A $\beta$  can activate microglial inflammasomes ([Halle et al., 2008](#)), activated inflammasomes are involved in the A $\beta$  deposition ([Heneka et al., 2013](#)), and inflammasome activation drives tau tangles ([Ising et al., 2019](#)), implicating a link among A $\beta$ , inflammasome activation, and development of amyloidopathy or tauopathy. It is interesting to note that the activated inflammasomes were detected in the cortex of A $\beta$ O-monkeys as in

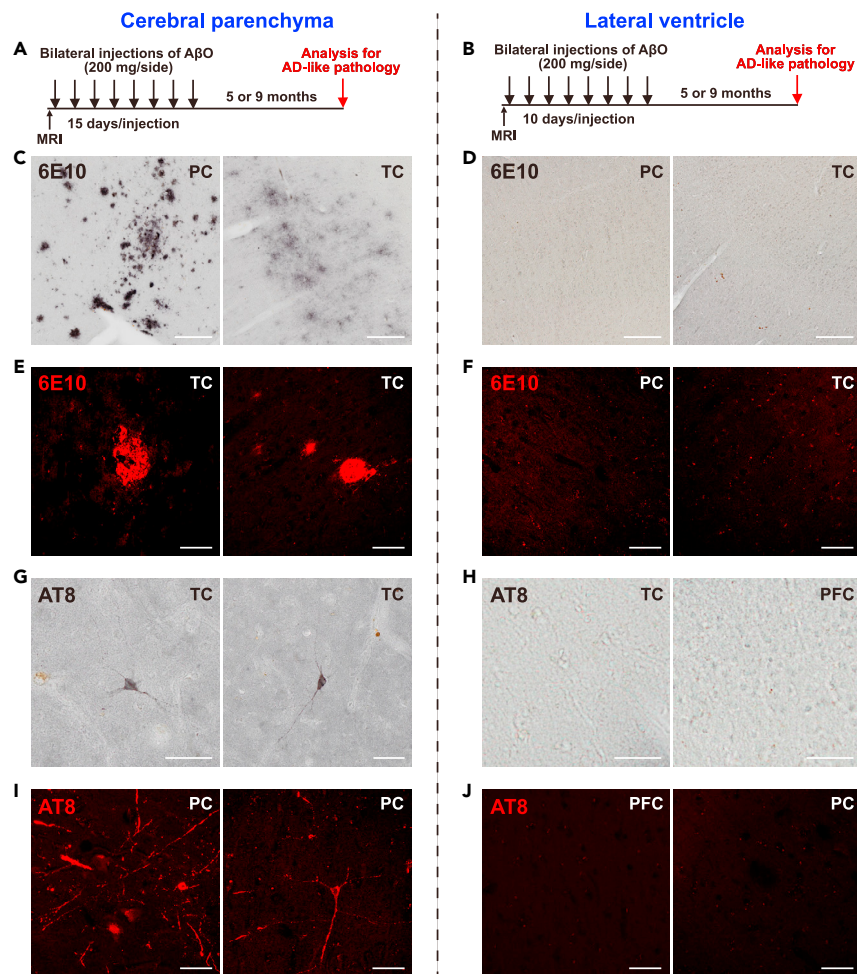


**Figure 7. The detection of amyloid and tau pathology in adult cynomolgus monkeys receiving intraparenchymal or intracerebroventricular delivery of A $\beta$ O**

(A) Schematic diagram of administration of A $\beta$ O in adult cynomolgus monkeys via intraparenchymal delivery (n = 3). Two monkeys had been treated for 5 months after the last A $\beta$ O injection, and one for 9 months.

(B) Schematic diagram of administration of A $\beta$ O in adult cynomolgus monkeys via intracerebroventricular delivery (n = 3). Two monkeys had been treated for 5 months after the last A $\beta$ O injection, and one for 9 months.

(C–F) Immunohistochemical (C and D) and immunofluorescent (E and F) analysis with 6E10 in whole brain sections from anterior to posterior cerebrum of intraparenchymal monkeys and representative brain regions with A $\beta$  plaques (C and E), as well as intracerebroventricular monkeys and representative brain regions without A $\beta$  plaques (D and F).

(G–J) Immunohistochemical (G and H) and immunofluorescent (I and J) analysis with AT8 in brain sections from anterior to posterior cerebrum of intraparenchymal monkeys and representative brain regions with tau tangles (G and I), as well as intracerebroventricular monkeys and representative brain regions without tau tangles (H and J). Abbreviations: PFC, prefrontal cortex; PC, parietal cortex; TC, temporal cortex. Scale bars: 200  $\mu$ m (C and D) and 50  $\mu$ m (E–J). See also [Figure S8](#) and [Table S2](#).

the cortex of patients with AD ([Figure S5](#)), suggesting that inflammasome might initiate A $\beta$ O-induced A $\beta$  deposition and subsequent tau tangles and contribute to rebuilding AD in cynomolgus monkey. Further exploration of these critical questions in the A $\beta$ O-monkeys would help to understand the crucial link between A $\beta$  deposition and tauopathy, the key juncture in the AD cascade, and eventually contribute to deciphering the pathogenesis of AD.

In this study, we observed some degenerative neurons in different brain regions and the tendency of neuronal loss in basal forebrain of A $\beta$ O-monkeys ([Figure 6](#)). Neurons in cortex and hippocampus with high A $\beta$  plaque burden in A $\beta$ O-induced cynomolgus brains appeared relatively intact. Although the

neuron loss is minor, the A $\beta$ O-monkeys displayed declined density of synapse associated with A $\beta$  plaques in some brain regions (Figure 6). Mounting evidences confirmed that the decreased synaptic density is the major neuropathological correlate of the degree of dementia in AD (Terry et al., 1991). The A $\beta$ -induced synaptic dysfunction and loss occurred at an early stage of AD, which led to failures of synaptic networks in AD brain directly causing cognitive deficits in patients (Davies et al., 1987; Palop and Mucke, 2010; Selkoe, 2002). The soluble A $\beta$ O were reported to induce impairments in synaptic integrity in the brain of rhesus monkeys (Beckman et al., 2019). The intranasal delivery of synthetic human A $\beta$ O impaired the long-term spatial memory of rat (Sipos et al., 2010). Although the behavioral effects of administering A $\beta$ O to monkeys remains unmeasured, these data imply the possibility of disrupting cognitive functions of cynomolgus monkeys by A $\beta$ O. Therefore, one of the next important steps will be to develop behavioral approaches suitable for cynomolgus monkeys, which allows one to measure the pattern of cognitive changes due to A $\beta$ O treatment. Then, we might interrogate the possibility of generating A $\beta$ O-monkeys with both typical pathologic features and the behavioral phenotypes that defines AD in humans. This will be evaluated in more detail in future studies.

In conclusion, we provided comprehensive characterization of cynomolgus monkeys receiving intraparenchymal delivery of synthetic A $\beta$ O and found that the progression of early AD was rapidly reproduced in the A $\beta$ O-monkeys. These results suggest that the A $\beta$ O-induced cynomolgus monkey might be a promising research model of human AD and would help advance our understanding of AD pathogenesis, which will eventually contribute to the development of promising research model for human AD.

### Limitations of the study

As already noted, the detected tau tangles in the brain of A $\beta$ O-monkeys were carefully characterized by most frequently used antibodies and standard techniques as shown in Figures 3, 4, and S2. Independent from the methods applied in our study, it is better to further confirm the conformation of tau tangles by other documented approaches, such as electron microscopy by using well-documented confirmational antibodies. We are planning to perform electron microscopic measurements in future studies.

### STAR★METHODS

Detailed methods are provided in the online version of this paper and include the following:

- KEY RESOURCES TABLE
- RESOURCE AVAILABILITY
  - Lead contact
  - Materials availability
  - Data and code availability
- EXPERIMENTAL MODEL AND SUBJECT DETAILS
  - Animals
- METHOD DETAILS
  - A $\beta$ O preparation
  - Intraparenchymal or intracerebroventricular delivery of synthetic A $\beta$ O
  - Immunostaining
  - Modified Bielschowsky's silver staining
  - Thioflavin S staining
  - Congo red staining
  - FJC staining
  - Western blot
  - Dot blot
- QUANTIFICATION AND STATISTICAL ANALYSIS
  - Counting analysis on brain slices
  - Statistical analysis

### SUPPLEMENTAL INFORMATION

Supplemental information can be found online at <https://doi.org/10.1016/j.isci.2021.103207>.

## ACKNOWLEDGMENTS

This work was supported in part by the National Key Basic Research and Development Program of China (2018YFA0108500, 2019YFA0801402, 2018YFA0800100, 2018YFA0108000, 2018YFA0107200, 2017YFA0102700), "Strategic Priority Research Program" of the Chinese Academy of Sciences, Grant No. (XDA16020501, XDA16020404), National Natural Science Foundation of China (81671224, 31472056, 31630043), and the Research Start-up Fund of Hainan University (RZ2100003016, RZ2000009939).

## AUTHOR CONTRIBUTIONS

F.Y. initiated the study and developed the methodology. S.F., C.L., and T.Z. performed the experiments and collected the data. S.F., T.Z., and C.Y. designed the experiments, analyzed the data, and made figures. C.L. and G.T. performed material preparation and stereotaxic surgeries. F.Y., C.Y., and N.J. conceived the study and interpreted results. C.Y. wrote the manuscript. N.J. supervised the study. All authors read and approved the final manuscript.

## DECLARATION OF INTERESTS

The authors declare no competing interests.

Received: August 11, 2020

Revised: August 4, 2021

Accepted: September 28, 2021

Published: October 22, 2021

## REFERENCES

- Augustinack, J.C., Schneider, A., Mandelkow, E.M., and Hyman, B.T. (2002). Specific tau phosphorylation sites correlate with severity of neuronal cytopathology in Alzheimer's disease. *Acta Neuropathol.* 103, 26–35.
- Baker, H.F., Ridley, R.M., Duchon, L.W., Crow, T.J., and Bruton, C.J. (1993). Evidence for the experimental transmission of cerebral beta-amyloidosis to primates. *Int. J. Exp. Pathol.* 74, 441–454.
- Beckman, D., Ott, S., Donis-Cox, K., Janssen, W.G., Bliss-Moreau, E., Rudebeck, P.H., Baxter, M.G., and Morrison, J.H. (2019). Oligomeric Aβeta in the monkey brain impacts synaptic integrity and induces accelerated cortical aging. *Proc. Natl. Acad. Sci. U. S. A.* 116, 26239–26246.
- Braak, H., and Del Tredici, K. (2015). Neuroanatomy and pathology of sporadic Alzheimer's disease. *Adv. Anat. Embryol. Cell Biol.* 215, 1–162.
- Brouillette, J., Cailliez, R., Zommer, N., Alves-Pires, C., Benilova, I., Blum, D., De Strooper, B., and Buée, L. (2012). Neurotoxicity and memory deficits induced by soluble low-molecular-weight amyloid-β1-42 oligomers are revealed in vivo by using a novel animal model. *J. Neurosci.* 32, 7852–7861.
- Caccamo, A., Branca, C., Piras, I.S., Ferreira, E., Huentelman, M.J., Liang, W.S., Readhead, B., Dudley, J.T., Spangenberg, E.E., Green, K.N., et al. (2017). Necroptosis activation in Alzheimer's disease. *Nat. Neurosci.* 20, 1236–1246.
- Choi, S.H., Kim, Y.H., Hebisch, M., Sliwinski, C., Lee, S., D'Avanzo, C., Chen, H., Hooli, B., Asselin, C., Muffat, J., et al. (2014). A three-dimensional human neural cell culture model of Alzheimer's disease. *Nature* 515, 274–278.
- Cramer, P.E., Gentzel, R.C., Tanis, K.O., Vardigan, J., Wang, Y., Connolly, B., Manfre, P., Lodge, K., Renger, J.J., Zerinatti, C., et al. (2018). Aging African green monkeys manifest transcriptional, pathological, and cognitive hallmarks of human Alzheimer's disease. *Neurobiol. Aging* 64, 92–106.
- Davies, C.A., Mann, D.M., Sumpter, P.Q., and Yates, P.O. (1987). A quantitative morphometric analysis of the neuronal and synaptic content of the frontal and temporal cortex in patients with Alzheimer's disease. *J. Neurol. Sci.* 78, 151–164.
- De Felice, F.G., Wu, D., Lambert, M.P., Fernandez, S.J., Velasco, P.T., Lacor, P.N., Bigio, E.H., Jerecic, J., Acton, P.J., Shughrue, P.J., et al. (2008). Alzheimer's disease-type neuronal tau hyperphosphorylation induced by Aβeta oligomers. *Neurobiol. Aging* 29, 1334–1347.
- Drummond, E., and Wisniewski, T. (2017). Alzheimer's disease: experimental models and reality. *Acta Neuropathol.* 133, 155–175.
- Edler, M.K., Sherwood, C.C., Meindl, R.S., Hopkins, W.D., Ely, J.J., Erwin, J.M., Mufson, E.J., Hof, P.R., and Raghanti, M.A. (2017). Aged chimpanzees exhibit pathologic hallmarks of Alzheimer's disease. *Neurobiol. Aging* 59, 107–120.
- Espuny-Camacho, I., Arranz, A.M., Fiers, M., Snellinx, A., Ando, K., Munck, S., Bonnefont, J., Lambot, L., Corthout, N., Omodho, L., et al. (2017). Hallmarks of Alzheimer's disease in stem-cell-derived human neurons transplanted into mouse brain. *Neuron* 93, 1066–1081.e1068.
- Fiandaca, M.S., Varenika, V., Eberling, J., McKnight, T., Bringas, J., Pivrotto, P., Beyer, J., Hadaczek, P., Bowers, W., Park, J., et al. (2009). Real-time MR imaging of adeno-associated viral vector delivery to the primate brain. *Neuroimage* 47, T27–T35.
- Forný-Germano, L., Lyra e Silva, N.M., Batista, A.F., Brito-Moreira, J., Gralle, M., Boehnke, S.E., Coe, B.C., Lablans, A., Marques, S.A., Martinez, A.M., et al. (2014). Alzheimer's disease-like pathology induced by amyloid-beta oligomers in nonhuman primates. *J. Neurosci.* 34, 13629–13643.
- Franklin, B.S., Latz, E., and Schmidt, F.I. (2018). The intra- and extracellular functions of ASC specks. *Immunol. Rev.* 281, 74–87.
- Geula, C., Wu, C.K., Saroff, D., Lorenzo, A., Yuan, M., and Yankner, B.A. (1998). Aging renders the brain vulnerable to amyloid beta-protein neurotoxicity. *Nat. Med.* 4, 827–831.
- Haass, C., and Selkoe, D.J. (2007). Soluble protein oligomers in neurodegeneration: lessons from the Alzheimer's amyloid beta-peptide. *Nat. Rev. Mol. Cell Biol.* 8, 101–112.
- Halle, A., Hornung, V., Petzold, G.C., Stewart, C.R., Monks, B.G., Reinheckel, T., Fitzgerald, K.A., Latz, E., Moore, K.J., and Golenbock, D.T. (2008). The NALP3 inflammasome is involved in the innate immune response to amyloid-beta. *Nat. Immunol.* 9, 857–865.
- Härtig, W., Klein, C., Brauer, K., Schüppel, K.F., Arendt, T., Brückner, G., and Bigl, V. (2000). Abnormally phosphorylated protein tau in the cortex of aged individuals of various mammalian orders. *Acta Neuropathol.* 100, 305–312.
- Heneka, M.T., Kummer, M.P., Stutz, A., Delekate, A., Schwartz, S., Vieira-Saecker, A., Griep, A., Axt, D., Remus, A., Tzeng, T.C., et al. (2013). NLRP3 is activated in Alzheimer's disease and contributes to pathology in APP/PS1 mice. *Nature* 493, 674–678.

- Ising, C., Venegas, C., Zhang, S., Scheiblich, H., Schmidt, S.V., Vieira-Saecker, A., Schwartz, S., Albasset, S., McManus, R.M., Tejera, D., et al. (2019). NLRP3 inflammasome activation drives tau pathology. *Nature* 575, 669–673.
- Kelley, N., Jeltama, D., Duan, Y., and He, Y. (2019). The NLRP3 inflammasome: an overview of mechanisms of activation and regulation. *Int. J. Mol. Sci.* 20, 3328.
- Koper, M.J., Van Schoor, E., Ospitalieri, S., Vandenberghe, R., Vandenbulcke, M., von Arnim, C.A.F., Tousseyn, T., Balusu, S., De Strooper, B., and Thal, D.R. (2020). Necrosome complex detected in granulovacuolar degeneration is associated with neuronal loss in Alzheimer's disease. *Acta Neuropathol.* 139, 463–484.
- Kwak, S.S., Washicosky, K.J., Brand, E., von Maydell, D., Aronson, J., Kim, S., Capen, D.E., Cetinbas, M., Sadreyev, R., Ning, S., et al. (2020). Amyloid- $\beta$ 42/40 ratio drives tau pathology in 3D human neural cell culture models of Alzheimer's disease. *Nat. Commun.* 11, 1377.
- LaFerla, F.M., and Green, K.N. (2012). Animal models of Alzheimer disease. *Cold Spring Harb. Perspect. Med.* 2, a006320.
- Lambert, M.P., Barlow, A.K., Chromy, B.A., Edwards, C., Freed, R., Liosatos, M., Morgan, T.E., Rozovsky, I., Trommer, B., Viola, K.L., et al. (1998). Diffusible, nonfibrillar ligands derived from A $\beta$ 1–42 are potent central nervous system neurotoxins. *Proc. Natl. Acad. Sci. U. S. A.* 95, 6448–6453.
- Lee, V.M., Goedert, M., and Trojanowski, J.Q. (2001). Neurodegenerative tauopathies. *Annu. Rev. Neurosci.* 24, 1121–1159.
- Lesné, S., Koh, M.T., Kotilinek, L., Kaye, R., Glabe, C.G., Yang, A., Gallagher, M., and Ashe, K.H. (2006). A specific amyloid- $\beta$  protein assembly in the brain impairs memory. *Nature* 440, 352–357.
- Lucin, K.M., and Wyss-Coray, T. (2009). Immune activation in brain aging and neurodegeneration: too much or too little? *Neuron* 64, 110–122.
- Malm, T., Ort, M., Tähtivaara, L., Jukarainen, N., Goldsteins, G., Puolivälä, J., Nurmi, A., Pussinen, R., Anttoniemi, T., Miettinen, T.K., et al. (2006). beta-Amyloid infusion results in delayed and age-dependent learning deficits without role of inflammation or beta-amyloid deposits. *Proc. Natl. Acad. Sci. U. S. A.* 103, 8852–8857.
- McLean, C.A., Cherny, R.A., Fraser, F.W., Fuller, S.J., Smith, M.J., Beyreuther, K., Bush, A.I., and Masters, C.L. (1999). Soluble pool of A $\beta$  amyloid as a determinant of severity of neurodegeneration in Alzheimer's disease. *Ann. Neurol.* 46, 860–866.
- Meyer-Luehmann, M., Spiess-Jones, T.L., Prada, C., Garcia-Alloza, M., de Calignon, A., Rozkalne, A., Koenigsnecht-Talboo, J., Holtzman, D.M., Bacskai, B.J., and Hyman, B.T. (2008). Rapid appearance and local toxicity of amyloid- $\beta$  plaques in a mouse model of Alzheimer's disease. *Nature* 451, 720–724.
- Oikawa, N., Kimura, N., and Yanagisawa, K. (2010). Alzheimer-type tau pathology in advanced aged nonhuman primate brains harboring substantial amyloid deposition. *Brain Res.* 1315, 137–149.
- Palop, J.J., and Mucke, L. (2010). Amyloid- $\beta$ -induced neuronal dysfunction in Alzheimer's disease: from synapses toward neural networks. *Nat. Neurosci.* 13, 812–818.
- Podlisny, M.B., Tolan, D.R., and Selkoe, D.J. (1991). Homology of the amyloid beta protein precursor in monkey and human supports a primate model for beta amyloidosis in Alzheimer's disease. *Am. J. Pathol.* 138, 1423–1435.
- Rosen, R.F., Farberg, A.S., Gearing, M., Dooyema, J., Long, P.M., Anderson, D.C., Davis-Turak, J., Coppola, G., Geschwind, D.H., Pare, J.F., et al. (2008). Tauopathy with paired helical filaments in an aged chimpanzee. *J. Comp. Neurol.* 509, 259–270.
- Rosen, R.F., Tomidokoro, Y., Farberg, A.S., Dooyema, J., Ciliax, B., Preuss, T.M., Neubert, T.A., Ghiso, J.A., LeVine, H., 3rd, and Walker, L.C. (2016). Comparative pathobiology of beta-amyloid and the unique susceptibility of humans to Alzheimer's disease. *Neurobiol. Aging* 44, 185–196.
- Sanfner, L.M., Sommer, J.M., Suzuki, B.M., Smith, P.H., Vijay, S., Vargas, J.A., Forsayeth, J.R., Cunningham, J., Bankiewicz, K.S., Kao, H., et al. (2005). AAV2-mediated gene delivery to monkey putamen: evaluation of an infusion device and delivery parameters. *Exp. Neurol.* 194, 476–483.
- Schagger, H. (2006). Tricine-SDS-PAGE. *Nat. Protoc.* 1, 16–22.
- Schmued, L.C., Albertson, C., and Slikker, W., Jr. (1997). Fluoro-Jade: a novel fluorochrome for the sensitive and reliable histochemical localization of neuronal degeneration. *Brain Res.* 751, 37–46.
- Schmued, L.C., Stowers, C.C., Scallet, A.C., and Xu, L. (2005). Fluoro-Jade C results in ultra high resolution and contrast labeling of degenerating neurons. *Brain Res.* 1035, 24–31.
- Selkoe, D.J. (2002). Alzheimer's disease is a synaptic failure. *Science* 298, 789–791.
- Selkoe, D.J., Bell, D.S., Podlisny, M.B., Price, D.L., and Cork, L.C. (1987). Conservation of brain amyloid proteins in aged mammals and humans with Alzheimer's disease. *Science* 235, 873–877.
- Sereno, M.I., and Tootell, R.B. (2005). From monkeys to humans: what do we now know about brain homologies? *Curr. Opin. Neurobiol.* 15, 135–144.
- Shankar, G.M., Li, S., Mehta, T.H., Garcia-Munoz, A., Shepardson, N.E., Smith, I., Brett, F.M., Farrell, M.A., Rowan, M.J., Lemere, C.A., et al. (2008). Amyloid- $\beta$  protein dimers isolated directly from Alzheimer's brains impair synaptic plasticity and memory. *Nat. Med.* 14, 837–842.
- Sipos, E., Kurunczi, A., Feher, A., Penke, Z., Fulop, L., Kasza, A., Horvath, J., Horvat, S., Veszelka, S., Balogh, G., et al. (2010). Intranasal delivery of human beta-amyloid peptide in rats: effective brain targeting. *Cell Mol. Neurobiol.* 30, 405–413.
- Stine, W.B., Jr., Dahlgren, K.N., Krafft, G.A., and LaDu, M.J. (2003). In vitro characterization of conditions for amyloid- $\beta$  peptide oligomerization and fibrillogenesis. *J. Biol. Chem.* 278, 11612–11622.
- Su, X., Kells, A.P., Salegio, E.A., Richardson, R.M., Hadaczek, P., Beyer, J., Bringas, J., Pivrotto, P., Forsayeth, J., and Bankiewicz, K.S. (2010). Real-time MR imaging with Gadoteridol predicts distribution of transgenes after convection-enhanced delivery of AAV2 vectors. *Mol. Ther.* 18, 1490–1495.
- Terry, R.D., Masliah, E., Salmon, D.P., Butters, N., DeTeresa, R., Hill, R., Hansen, L.A., and Katzman, R. (1991). Physical basis of cognitive alterations in Alzheimer's disease: synapse loss is the major correlate of cognitive impairment. *Ann. Neurol.* 30, 572–580.
- Viola, K.L., and Klein, W.L. (2015). Amyloid beta oligomers in Alzheimer's disease pathogenesis, treatment, and diagnosis. *Acta Neuropathol.* 129, 183–206.
- Walker, L.C., and Jucker, M. (2017). The exceptional vulnerability of humans to Alzheimer's disease. *Trends Mol. Med.* 23, 534–545.
- Walsh, D.M., Tseng, B.P., Rydel, R.E., Podlisny, M.B., and Selkoe, D.J. (2000). The oligomerization of amyloid beta-protein begins intracellularly in cells derived from human brain. *Biochemistry* 39, 10831–10839.
- Weiner, H.L., and Frenkel, D. (2006). Immunology and immunotherapy of Alzheimer's disease. *Nat. Rev. Immunol.* 6, 404–416.
- Wyss-Coray, T., and Mucke, L. (2002). Inflammation in neurodegenerative disease—a double-edged sword. *Neuron* 35, 419–432.
- Zheng, J., Li, H.-L., Tian, N., Liu, F., Wang, L., Yin, Y., Yue, L., Ma, L., Wan, Y., and Wang, J.-Z. (2020). Interneuron accumulation of phosphorylated tau impairs adult hippocampal neurogenesis by suppressing GABAergic transmission. *Cell Stem Cell* 26, 331–345.

## STAR★METHODS

### KEY RESOURCES TABLE

| REAGENT or RESOURCE                                  | SOURCE  | IDENTIFIER  |
|--|---|---|
| <b>Antibodies</b>                                    |   |   |
| Mouse anti-A $\beta$ <sub>1-16</sub> (6E10)          | Covance                                       | Cat # SIG-39320; RRID: AB_662798  |
| Mouse anti-A $\beta$ <sub>17-24</sub> (4G8)          | Biolegend                                     | Cat # SIG-39220; RRID: AB_662812  |
| Rabbit anti-Amyloid Fibrils OC                       | Sigma-Aldrich                                 | Cat # AB2286; RRID: AB_1977024  |
| Mouse anti-PHF-tau (Ser202, Thr205) (AT8)            | Thermo Fisher Scientific                      | Cat # MN1020; RRID: AB_223647   |
| Mouse anti-phospho-Tau (Thr212, Ser214) (AT100)      | Thermo Fisher Scientific                      | Cat # MN1060; RRID: AB_223652   |
| Rabbit anti-NF-H                                     | Proteintech                                   | Cat # 21471-1-AP; RRID: AB_10734324   |
| Rabbit anti-GFAP                                     | Abcam   | Cat # ab16997; RRID: AB_443592  |
| Rabbit anti-Iba1                                     | Wako  | Cat # 019-19741; RRID: AB_839504  |
| Goat anti-Iba1                                       | Abcam   | Cat # ab5076; RRID: AB_2224402  |
| Rabbit anti-NEUN                                     | Millipore                                     | Cat # ABN78; RRID: AB_10807945  |
| Goat anti-ChAT                                       | Millipore                                     | Cat # AB144P; RRID: AB_2079751  |
| Rabbit anti-ASC                                      | AdipoGen                                      | Cat # AG-25B-0006; RRID: AB_2490440   |
| Mouse anti-Caspase1                                  | AdipoGen                                      | Cat # AG-20B-0048; RRID: AB_2490257   |
| Rabbit anti-Synaptophysin                            | Abcam   | Cat # ab32127; RRID: AB_2286949   |
| Rabbit anti-pMLKL (S358)                             | Abcam   | Cat # ab187091; RRID: AB_2619685  |
| Alexa Fluor® 594 AffiniPure Fab Fragment             | Jackson ImmunoResearch                        | Cat # 715-587-003; RRID: AB_2340859   |
| Donkey Anti-Mouse IgG (H+L)                          |   |   |
| Normal mouse serum                                   | Jackson ImmunoResearch                        | Cat # 015-000-120; RRID: AB_2337194   |
| Normal donkey serum                                  | Jackson ImmunoResearch                        | Cat # 017-000-121; RRID: AB_2337258   |
| <b>Chemicals, peptides, and recombinant proteins</b> |   |   |
| Human A $\beta$ <sub>1-42</sub> peptide              | Chinese Peptide                               | Cat # AMYD-003  |
| HFIP   | Sigma-Aldrich                                 | Cat # 105228  |
| DMSO   | Sigma-Aldrich                                 | Cat # D8418   |
| HEPES  | Sigma-Aldrich                                 | Cat # H4034   |
| Fluoro-Jade C  | Millipore                                     | Cat # AG325   |
| Thioflavin S   | Sigma-Aldrich                                 | Cat # T1892   |
| Congo Red  | Sigma-Aldrich                                 | Cat # C6277   |
| <b>Critical commercial assays</b>                    |   |   |
| BCA assay kit  | Thermo Fisher Scientific                      | Cat # 23225   |
| ECL western blotting substrate                       | Thermo Fisher Scientific                      | Cat # 32209   |
| VECTASTAIN ABC Reagent kit                           | Vector Labs                                   | Cat # PK-4000   |
| VECTOR DAB Substrate Kit                             | Vector Labs                                   | Cat # SK-4100   |
| Modified Bielschowsky's Stain Kit                    | American MasterTech                           | Cat # KTBIE   |
| <b>Experimental models: Organisms/strains</b>        |   |   |
| Macaca fascicularis animals                          | Wincon Theracells<br>Biotechnologies Co, LTD. | N/A   |
| <b>Software and algorithms</b>                       |   |   |
| ImageJ   | ImageJ  | <a href="https://imagej.nih.gov/ij/download.html">https://imagej.nih.gov/ij/download.html</a>                         |
| Graphpad Prism 6                                     | GraphPad Software                             | <a href="https://www.graphpad.com/scientific-software/prism/">https://www.graphpad.com/scientific-software/prism/</a> |
| StrataQuest software version 6.0.1.145               | TissueGnostics, Vienna, Austria               | N/A   |

(Continued on next page)

**Continued**

| REAGENT or RESOURCE  | SOURCE   | IDENTIFIER  |
|--|----------|-------------|
| Other  |          |             |
| 250 $\mu$ L Gastight Syringe Model 1725 LTN, Cemented Needle, 22s gauge, 2 in, point style 2 | Hamilton | Cat # 81100 |
| Microtome  | Leica    | SM2000R     |
| VS120 Virtual Slide Microscope   | Olympus  | VS120       |
| Confocal laser scanning microscope   | Leica    | TCS SP8     |

**RESOURCE AVAILABILITY****Lead contact**

Further information and requests for resources and reagents should be directed to and will be fulfilled by the lead contact, Naihe Jing ([njing@sibcb.ac.cn](mailto:njing@sibcb.ac.cn)).

**Materials availability**

This study did not generate new unique reagents.

**Data and code availability**

- All data reported in this paper will be shared by the lead contact upon request.
- This paper does not report original code.
- Any additional information required to reanalyze the data reported in this paper is available from the lead contact upon request.

**EXPERIMENTAL MODEL AND SUBJECT DETAILS****Animals**

The care of non-human primates and procedures involved in this study were thoroughly reviewed and approved by the Animal Care and Use Committee, in accordance with the Association for Reassessment and Accreditation of Laboratory Animal Care (AAALAC) guideline.

Fourteen cynomolgus monkeys (*Macaca fascicularis*) aged 18–22 years were recruited in the first experiment of this study and randomly assigned to two groups, A $\beta$ O-induced group ( $n = 7$ , 5 females and 2 males) and noninjected control group ( $n = 7$ , 6 females and 1 male) as shown in [Table S1](#). Another six cynomolgus monkeys aged 20–24 years were recruited in the second experiment of this study and randomly assigned to two groups, A $\beta$ O-intracerebroventricular delivery group ( $n = 3$ , 2 females and 1 male) and A $\beta$ O-intrapancreatic delivery group ( $n = 3$ , 2 males and 1 female) as shown in [Table S2](#). All these 20 monkeys are wild type animals from the same colony and had never been involved in other pharmacological trials and studies. During the study, animals were individually housed in stainless steel cages at the primate facility of Wincon Theracells Biotechnologies Co, LTD. in Nanning, Guangxi China, which is fully accredited by the AAALAC International. Animals are fed twice daily and supplemented with fresh fruits and the miscellaneous enrichments once a day. All animals are maintained on a 12-h light and/or 12-h dark cycle under room temperature at 22–28°C with a relative humidity of 30%–75% and water supply ad libitum.

**METHOD DETAILS****A $\beta$ O preparation**

Human A $\beta$ <sub>1–42</sub> peptide was commercially synthesized by Chinese Peptide. We adopted and modified the procedures as previously described for the oligomerization of A $\beta$  peptides ([Stine et al., 2003](#)). Briefly, 1 mg lyophilized peptide stored at –80°C was allowed to equilibrate to room temperature for 30 min. Then, the peptide was thoroughly dissolved to 1 mM in 100% 1,1,1,3,3,3-Hexafluoro-2-propanol (HFIP, Sigma). The solution containing the dissolved peptide was then aliquoted in microcentrifuge tubes. The solution was subjected to a gentle stream of nitrogen to evaporate HFIP and a thin clear film at the bottom of the tube was produced. During evaporation, approximately 30–50% of A $\beta$  was lost. The evaporated peptide was subsequently resuspended in 40  $\mu$ l dimethyl sulfoxide (DMSO) and further diluted in 10 mM HEPES

to a final concentration of 110  $\mu\text{M}$ . The oligomers were freshly prepared before each injection and were characterized by western blot. The A $\beta$ O can be kept on ice for at most 5 h before injection. Vehicle controls were prepared in an identical manner using the same tubes and solutions in the absence of A $\beta$ 1-42 peptide.

### **Intraparenchymal or intracerebroventricular delivery of synthetic A $\beta$ O**

For the brain administration of A $\beta$ O, four MRI-guided stereotaxic surgeries combined with convection enhanced delivery system (Fiandaca et al., 2009; Sanftner et al., 2005) were performed on each cynomolgus monkey as shown in Figure 1A. Each monkey was anesthetized with intramuscular atropine (20 mg/kg), ketamine (10 mg/kg), and sodium pentobarbital (20 mg/kg). The head of the monkey was fixed in a stereotaxic instrument and the skull over the parietal lobe was exposed under aseptic conditions by a longitudinal skin incision followed by removal of the connective tissue. MRI scanning was performed on each monkey prior to surgery to identify stereotaxic coordinates. A small hole (<2 mm in diameter) on the skull of each side of brain was made using an electric drill guided by parameters from MRI measurements. The A $\beta$ O solution (0.5  $\mu\text{g}/\mu\text{l}$ ) was bilaterally injected into the brain parenchyma between the lateral basal ganglia and medial temporal lobe directly above the hippocampus or lateral ventricles using Hamilton syringes (gauge 22s). The needle was pushed into the target location at a rate of 1 mm/min through the small hole and held in place for 10 min. Then, 200  $\mu\text{l}$  volume of A $\beta$ O was injected into each side of brain at a rate of 2  $\mu\text{l}/\text{min}$ . The needles were held in place for 20 min following A $\beta$ O delivery and then drawn back at a rate of 1 mm/min. For each animal, four A $\beta$ O injections (800  $\mu\text{l}$  per side) were performed at 6~8-week intervals as shown in Figure 1.

To verify the injection accuracy and predict A $\beta$ O diffusion in cynomolgus cerebrum, two animals received a bilateral intra-brain injection of soluble A $\beta$ O containing contrast agent, gadopentetate dimeglumine (Gd-DTPA), following the same surgery protocol as the A $\beta$ O injection (Su et al., 2010). An MRI scanning was performed 2 h after surgery to detect the Gd-DTPA signal.

### **Immunostaining**

Animals were perfused with saline under deep anesthesia with sodium pentobarbital (30 mg  $\text{kg}^{-1}$  intravenously). Brains were coronally cut into 4–6 mm thick sections before fixation with 4% paraformaldehyde for 3 days at 4°C. These thick sections were then washed with PBS three times and sequentially transferred to 15% and 30% sucrose solution at 4°C. The thick sections were further cryosectioned at 40- $\mu\text{m}$  thickness using a microtome (Leica SM2000R) and stored in ethylene glycol solutions at –20°C. In some cases, before fixation of the thick sections, small samples of various regions were obtained and flash frozen at –80°C for subsequent immunoblot analysis.

For immunohistochemistry (IHC) assays, the brain sections of 40- $\mu\text{m}$  thickness were washed with PBS three times and quenched of endogenous peroxidase activity in 0.3%  $\text{H}_2\text{O}_2$  in PBS for 30 min. After permeabilization and blocking in the 10X blocking buffer containing 5% donkey normal serum, 1% BSA, and 0.4% Triton X-100 for 2 h, the sections were incubated in primary antibody diluted with 1X blocking buffer for 16 h at 4°C. The primary antibodies used were as follows: anti-A $\beta$ <sub>1-16</sub> (6E10) (BioLegend, 1:1000), anti-A $\beta$ <sub>17-24</sub> (4G8) (BioLegend, 1:1000), anti-PHF-tau (Ser202, Thr205) (AT8) (Thermo Fisher Scientific, 1:1000), anti-phospho-Tau (Thr212, Ser214) (AT100) (Thermo Fisher Scientific, 1:1000), anti-Iba1 (Wako, 1:1000), anti-GFAP (Abcam, 1:1000) and anti-ChAT (Millipore, 1:1000). After washing in PBS between steps, brain sections were incubated in species-appropriate biotinylated secondary antibody (e.g., donkey anti-mouse IgG (H + L) biotin secondary antibody or donkey anti-rabbit IgG (H + L) biotin secondary antibody) for 2 h at room temperature. After 3 washes with PBS, the sections were then transferred to the avidin-biotin-peroxidase complex (prepared from VECTASTAIN ABC Reagent kit) for 30 min, and then reacted with DAB-hydrogen peroxide solution (prepared from VECTOR DAB Substrate Kit). In some circumstances,  $\text{NiSO}_4$  was added to amplify the signal. The sections were then washed with PBS, mounted on slides, dehydrated in increasing concentrations of ethanol, cleared in xylenes, and coverslipped using neutral resins.

For immunofluorescent staining, the primary antibodies used were as follows: anti-A $\beta$ <sub>1-16</sub> (6E10) (BioLegend, 1:500), anti-A $\beta$ <sub>17-24</sub> (4G8) (BioLegend, 1:200), anti-PHF-tau (Ser202, Thr205) (AT8) (Thermo Fisher Scientific, 1:400), anti-NF-H (Proteintech, 1:800), anti-Iba1 (Wako, 1:500), anti-Iba1 (Abcam, 1:500), anti-GFAP (Abcam, 1:200), anti-pMLKL (Abcam, 1:100), anti-NEUN (Millipore, 1:500), anti-ASC (AdipoGen, 1:200) and anti-Synaptophysin (Abcam, 1:1000). Fluorescent staining with species-appropriate Alexa secondary antibodies (Jackson ImmunoResearch Laboratories) was used. To reduce the autofluorescence in

fluorescently labeled brain tissue, the brain sections were dipped briefly in distilled water, and treated with 5 mM CuSO<sub>4</sub> in 50 mM ammonium acetate buffer (pH 5.0) for 30 min. The brain sections were then counterstained with DAPI (Sigma), mounted on slides, and coverslipped in Fluoromount-G (Thermo Fisher Scientific).

For co-staining of 6E10 and AT8 on the brain sections, the multiple mouse-on-mouse staining protocol were performed as previously described (Koper et al., 2020). Since the two antibodies are originated from the same host species, coupling method was used to avoid cross-reactivity of secondary antibodies. Briefly, AT8 was stained as described above, followed by the Alexa Fluor® 488 donkey anti-mouse secondary antibody, while 6E10 was coupled to a donkey anti-mouse Fab fragment conjugated to Alexa 594 (Jackson ImmunoResearch). For coupling of 6E10, the antibody was incubated with the Fab fragment for 40 min at RT (2 µg Fab fragment per 1 µg 6E10). Normal mouse serum was then added to capture the unbound Fab fragment (10 µl of serum per 1 µg Fab fragment) for another 20 min. The coupled 6E10 antibody was subsequently used to stain the brain sections, following the standard protocol described above.

For collecting images, a fully automated and high-resolution scanning system, VS120 Virtual Slide Microscope (Olympus), was used to scan the whole brain slides.

### Modified Bielschowsky's silver staining

To further identify the intracellular neurofibrillary tangles, modified Bielschowsky's silver staining was performed using a Modified Bielschowsky's Stain Kit (American MasterTech). Ammoniacal silver solution, developer solution and ammonia water were prepared according to the kit procedure. 40-µm free-floating brain sections were mounted on slides and then rinsed in distilled water. Place the slides in preheated silver nitrate solution for 15 min at 40°C. After 3 washes with distilled water, treat the slides with preheated ammoniacal silver solution for 10 min at 40°C. Slides were immersed in developer solution for 3–30 sec until the tissue became golden brown and removed quickly into ammonia water for 30 sec. Slides were rinsed in running distilled water and then treated with 5% sodium thiosulfate for 2 min. After wash in running distilled water for 2 min, the slides were dehydrated in absolute alcohol, cleared in xylenes, and coverslipped using neutral resins.

### Thioflavin S staining

Free-floating brain sections were washed with PBS for 3 × 5 min, then mounted on the slides and dried. The slides were then incubated with 0.025% Thioflavin S (dissolved in 50% ethanol) at room temperature for 8 min. The slides were then decolorized in 50% ethanol for 2 × 1 min, washed in PBS, and subsequently co-stained with DAPI and coverslipped using Fluoromount-G. Images were captured with Leica TCS SP8 confocal laser scanning microscope.

### Congo red staining

Congo red staining was performed as previously described (Zheng et al., 2020). Briefly, free-floating brain sections were washed with PBS for 3 × 5 min, then mounted on the slides and dried. The slides were incubated in a sodium chloride solution (3% NaCl, 80% ethanol and 0.01% NaOH) at room temperature for 20 min, and then 0.2% Congo red containing 3% NaCl, 80% ethanol and 0.01% NaOH for 40 min. The sections were subsequently decolorized in ethanol, cleared in xylenes, and coverslipped using neutral resins.

### FJC staining

Fluoro-Jade C staining is used to visualize degenerated neurons on 40-µm Macaque brain sections as previously described (Schmued et al., 2005). Following standard immunostaining using Aβ<sub>1-16</sub> antibody 6E10 and Alexa594-conjugated secondary antibody, the sections were mounted onto premier charged slides and dried at 50° for 30 min. They were rinsed with distilled water and then dipped in 0.06% potassium permanganate solution for 5 min. After a 2-min water rinse, the slides were incubated with 0.0004% FJC in 0.1% acetic acid for 20 min. The slides were then stained with DAPI and coverslipped using Fluoromount-G. Images were captured with Leica TCS SP8 confocal laser scanning microscope.

### Western blot

To characterize the Aβ species in the oligomerized Aβ<sub>1-42</sub> peptide, the AβO sample was electrophoresed on 16% acrylamide Tricine-SDS-PAGE gels and transferred onto 0.2 µm PVDF membranes at 30 V for 2 h

(Schagger, 2006). Filters were boiled for 5 min in PBS and blocked at room temperature for 1 h with 5% fat-free milk in PBS. Monoclonal antibody 6E10 (1:2000) was used to probe the blots. Bound antibody was visualized using HRP-conjugated anti-mouse IgG (1:7000) (Abcam) and ECL detection (Thermo Fisher Scientific).

For detection of A $\beta$  in brain tissue samples from cynomolgus monkeys, tissues were homogenized in RIPA buffer containing protease and phosphatase inhibitors (50 mM Tris-HCl (pH7.6), 150 mM NaCl, 0.1% SDS, 1% NP40, 1 mM EDTA, 1 mM EGTA, 1% deoxycholic acid sodium salt, 1 mM DTT, 1 mM PMSF, 1 mM NaF, 1 mM Na<sub>3</sub>VO<sub>4</sub>, 1  $\mu$ g/ml leupeptin, 1  $\mu$ g/ml aprotinin, and 1  $\mu$ g/ml pepstatin) and then rotated at 4°C for 30 min. The homogenates were then centrifuged for 30 min at 4°C, 12,000 rpm. The protein concentration of supernatant was measured by BCA assay. The resulting pellet was resuspended with 2% SDS in 25 mM Tris-HCl (pH7.5), centrifuged again, and the supernatant was collected as the detergent-insoluble fraction of the brain samples. These samples were then diluted in SDS sample buffer and resolved on a 4% stacking gel and 10% separating gel containing 6 M urea in Tricine-SDS buffer. The gel was transferred onto 0.2  $\mu$ m PVDF membrane and the western blot was performed following the same protocol as for A $\beta$ O samples described above. The membrane was probed with 6E10 and anti- $\beta$ -actin antibody, the latter serving as a loading control.

For immunoblot detection of Caspase1, the supernatant samples were diluted in SDS sample buffer and separated by 12% SDS-PAGE gels. The proteins were transferred onto 0.45  $\mu$ m PVDF membranes at 100 V for 2 h. The membranes were then blocked in 3% BSA in TBS for 1 h at room temperature followed by incubation of anti-Caspase1 (AdipoGen, 1:1000) in 3% BSA in TBS-Tween overnight at 4°C. The membrane was also visualized using HRP-conjugated anti-mouse IgG and ECL detection. Signal intensities were quantified by ImageJ software.

### Dot blot

The A $\beta$ O aliquots (1  $\mu$ l) were spotted on a nitrocellulose membrane (Pierce). The membrane was blocked for 1 hour at room temperature with 10% nonfat milk in Tris-buffered saline containing 0.01% Tween 20 (TBS-T) and probed with 6E10 (1:10000 in 3% BSA), 4G8 (1:10000 in 3% BSA), OC (1:1000 in 5% nonfat milk). HRP-conjugated anti-mouse/rabbit IgG secondary antibodies (Abcam) were used at 1:5000 for 1 h at room temperature. Blots were detected using ECL chemiluminescence detection reagent (Thermo Fisher Scientific).

## QUANTIFICATION AND STATISTICAL ANALYSIS

### Counting analysis on brain slices

For counting analysis, image processing of whole brain sections (for A $\beta$  plaques) or specific brain regions (for astrocytes, microglia, synaptic dots and neurons) and analysis was performed using StrataQuest software version 6.0.1.145 (TissueGnostics, Vienna, Austria). The quantification of A $\beta$  plaques were performed on four serial whole brain sections from the anterior to posterior of each cynomolgus cerebrum. For quantifying astrocytes, microglia and synaptic dots, three fields on each cortical region were randomly selected and at least two cortical regions of each cynomolgus cerebrum were measured.

### Statistical analysis

All of the statistical details of experiments can be found in the figure legends. All data are presented as mean  $\pm$  SEM. Student's *t* test (two-tailed) was performed for statistical analysis between two groups. A value of *p* < 0.05 was considered significant in all analyses. All statistical analyses were conducted using Prism 6 GraphPad Software (San Diego, CA).